Universidad Politécnica de Madrid

Escuela Técnica Superior de Ingenieros Industriales

Departamento de Automática, Ingeniería Electrónica e Informática Industrial

Máster Universitario en Electrónica Industrial

A Low-Cost Piezoelectric Human Energy Harvester for Smart Cities and Wireless Sensor Networks

Autor: David Butkiewicus

Tutores: Pedro Alou y Teresa Riesgo

Junio, 2014

Trabajo Fin de Máster

EAGLES Program

Índice

Abstract

A major hurdle in building "smart cities" is providing the framework for real-time data collection and analysis, which is subsequently used to react to changing conditions in order to maintain the operation or efficiency of a given city's system. Ideally, these data collection nodes should operate independently and indefinitely. This implies that these data collection nodes need to scavenge their own power from the many sources available in the environment. This thesis work culminated in the construction, testing, and implementation study of a prototype piezoelectric energy harvester for human foot traffic using THUNDER 7R piezoelectric actuators to power a Cookie wireless sensor network (WSN) node. After the actuators were tested, the power conditioning circuitry was designed in parallel to the development of the mechanical enclosure. The system was then modeled using PSPICE, and this same model was used to explore the power output with numerous actuators—only 1 Thunder 7R actuator was available for testing after the other was destroyed during a trial run. It was found that for 10 seconds of constant human traffic flow (with footfall at a rate of 1.5 Hz), one actuator can produce about 1.25 mJ of energy. Every actuator that is added in parallel will contribute another 1.25 mJ, and this harvester is easily scalable since these Thunder actuators can be stacked on top of one another. In the implementation study, it was found that there is enough power with a few of these actuators to power a Cookie WSN node for a variety of applications, even though these nodes were designed specifically for flexibility rather than low power consumption. The total cost of a dual-actuator harvester was well under €300, which is significantly cheaper than the human footstep harvesting solutions available on the market today. Although this harvester does not produce nearly as much energy as the aforementioned electromagnetic-based commercial harvesters, it can fill a niche in the WSN harvester market since it offers a low-cost, easily scalable, durable system that can provide enough energy in high-traffic locations for low-power sensor nodes such as the WaspMote or the TelosB platform.

Introduction

As urban populations grow, it becomes increasingly difficult for a given city's infrastructure to efficiently keep up with an expanding workload. A major part of this problem is that it's a rare occurrence for city planners to have sufficient data to make informed decisions as well as the fact that the city's existing infrastructure cannot easily adapt real-time to varying conditions. It would be prohibitively costly as well as inefficient to train a staff to log and tweak current infrastructure conditions in order to improve the overall efficiency of a given subsystem in a city. An attractive solution to these issues is to create a network of autonomous sensors that can communicate with one another or a common arbiter (depending on the configuration). Wireless Sensor Networks (WSNs) are specific types of robust networks that are becoming more and more ubiquitous each year due to the interest in Smart Cities and sustainability. The basic attribute of a WSN is that is consists of many nodes that can relay information amongst each other in a given environment. The nodes typically consist of a wireless transceiver, microprocessor, sensors, energy storage units, and energy harvesting units (if no external power is available or desired). The nodes can be arranged in a variety of configurations, such as star topologies or multi-hop mesh networks. Advanced WSNs can also reconfigure themselves seamlessly if nodes are moving or become nonoperational. They are very useful in applications such as environmental monitoring (forest fire detection, air quality, temperature, etc.), surveillance, sensor banks, and military applications, amongst others.

The ultimate goal for a node in a WSN is for it to be completely self-sufficient and independent, meaning it does not need any external power or humans to maintain it. Once installed, the node should be able to perform its various tasks autonomously without any external assistance. In order attain this goal the node has to be capable of harvesting energy from its environment.

Whether or not it's obvious to us, we are surrounded by sources of energy. From the sunlight to the wind, from vibrations to radio waves, there exists energy that can be transformed into usable electrical power. The most important questions to ask are: how efficient are these various energy conversion methods, and what solution (or combination of solutions) make the most sense for this specific application? Table 1 below shows a comparison of various energy transformation methods. From this table, it is obvious that solar energy offers the advantages of very high energy output when it is sunny, as well as resistance to aging. This assumes, of course, that the solar panels are properly maintained. A common issue is that when the panels get dirty, its output is significantly decreased. One can see that batteries degrade by about a

factor of 10 over ten years. Nuclear isotopes are not a viable option due to safety and environmental concerns, perhaps nuclear energy sources would not be appropriate for anything but a specific military application. The two scavenged sources that utilize piezoelectric harvesting are the shoe inserts and vibrations, which can create more than enough energy to operate a node if the conditions are favorable.

Type of Source	Energy Type	Power Density (uW/cm^3) for 1 Year Lifetime	Power Density (uW/cm^3) for 10 Year Lifetime
Scavenged Sources	Solar (Outdoors)	15,000 (sunny day)	15,000 (sunny day)
		150 (cloudy day)	150 (cloudy day)
	Solar (Indoors)	6 (office desk)	6 (office desk)
	Vibrations	200	200
	Acoustic Noise	0.003 @ 75 dB	0.003 @ 75 dB
		0.96 @ 100 dB	0.96 @ 75 dB
	Daily Temp. Δ	10	10
	Temp. Gradient	15 @10°C gradient	15 @10°C gradient
	Shoe Inserts	330	330
Energy Reservoirs	Rechargable Lithium Battery	45	3.5
	Non-Rechargable Lithium Battery	7	0
	Hydrocarbon Fuel (micro-heat oven)	333	33
	Fuel Cell (methanol)	280	28
	Nuclear Isotopes (uranium)	6×10^6	6×10^5

Table 1- Comparison of energy sources [1]

Motivation

This thesis project was envisioned after completing a master's course in Wireless Sensor Networks (WSNs) at Universidad Politécnica de Madrid and learning about the exciting prospects and unique problems that are inherent to Smart City/WSN initiatives. After researching the current state of energy harvesting technologies (more specifically human footfall harvesting), it became evident that the existing solutions are almost prohibitively costly, require a significant amount of work to install and maintain, and need to be catered to each specific installation site. This research instilled the realization that there needs to be a cheaper, more flexible solution for harvesting human footfall in areas where other renewable resources do not make sense. Additionally, the popular notion that this harvester has to generate as much power as possible was abandoned—this increases price and complexity, and with the advent of mobile technologies and WSNs the market is flooded with ultra-low power sensors, processors, and communication modules. The design philosophy here was to find a happy medium between price, flexibility, and ability. For example, if a WSN node is only being used to send sensor information once every x minutes (and is in a very low-power sleep state otherwise), it can be self-sufficient with the proper planning and energy management algorithms. These goals and more were explored for this thesis work.

Theory

I. Mechanical Harvesting

Mechanical harvesters take advantage of the fact that there are forms of mechanical perturbations all around our industrial and natural world. Figure 1 shows a typical office building and the various frequencies and sources of harvestable mechanical energy. Most of the vibrations we experience on a daily basis are in the 1-100 Hz range. The most common sources of these vibrations are appliances, traffic, microwaves, etc. Frequencies higher than this can be found inside cars and industrial buildings, where some motors can generate frequencies over 1000 Hz.

There are three different approaches one can take in order to harvest these external vibrations. They are piezoelectric conversion, electrostatic conversion, and magnetic induction conversion.

- *Piezoeletric converters* utilize piezoelectric materials to convert a mechanical stress or strain into an electric field, which can then be captured using transducers. This method produces the highest energy density of the 3 choices.
- *Electrostatic converters* use 2 conductors separated by a compressible dielectric, which forms a capacitor. When this structure encounters a mechanical force, it will compress and increase the energy stored by decreasing the effective dielectric width. This technology is well-suited to foot and road traffic, but has a distinct disadvantage of having to be charged externally first. Perhaps this could work in tandem with a solar cell for a remote WSN node. An advantage of this approach is that it creates high voltages, which can be easily rectified into AC.
- *Electromagnetic converters* are constructed with a coil and a moving magnetic mass. As Farady's law dictates, a moving magnetic field in a conductor will induce a current. There are a variety of ways to exploit this effect, one example that you might have used in real life is the flashlights that can recharge by shaking it along an axis. There is a cylindrical magnet enclosed in a tube that is wrapped in a coil. As the flashlight is shaken, the magnet moves rapidly back and forth through the tube, inducing a current in the coil which is then stored in either a capacitor or battery. One disadvantage of this method is that low voltages are produced, which makes it difficult to rectify.

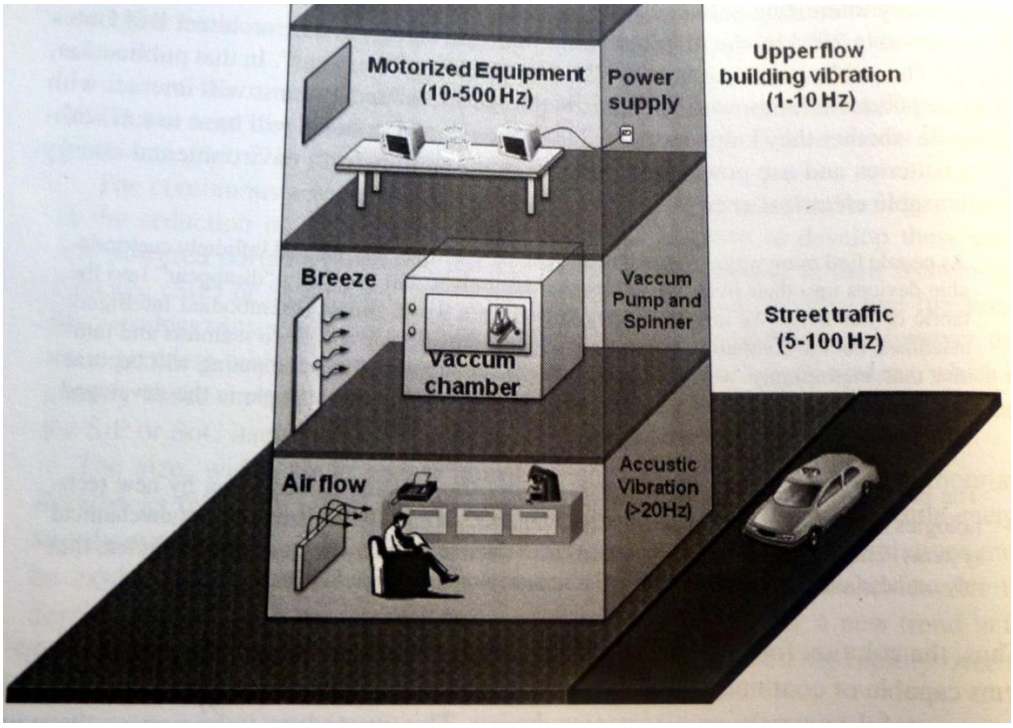

Figure 1- Various sources of vibrations around an office building. [1]

Type	Governing Equation	Practical Max (mJ/cm^3)	Theoretical Max
Piezoelectric	$u = \sigma_y^2 k^2/2Y$	17.7	335 mJ/cm^3
Electrostatic	$u = 0.5\varepsilon E^2$	4	44 mJ/cm^3
Electromagnetic	$B^2/2\mu_0$	4	400 mJ/cm^3

Table 2- Comparison of energy densities for mechanical harvesting. [1]

Table 2 shows a comparison of the maximum energy densities; piezoelectric harvesting is capable of the greatest in practical use. Choosing which approach best satisfies the node requirements is a matter of defining the conditions. Questions that should arise include "What kind of energy is available?", "What are the physical limitations?", or "Is there any commercially available product that will suit my design, or is a custom converter be the only option?". In this case, piezoelectric-

based converters will be explored due to their suitability to human traffic harvesting as well as the fact that there are many commercial piezoelectric converters available.

II. Piezoelectric Effect

This paper will focus on piezoelectric energy harvesters. These types of harvesters utilize the inherent trait of piezoelectric materials, which is that mechanical forces induce electric fields in the material. This works inversely as well—an electric field will cause mechanical disturbances, which are classified into two categories: stress and strain.

The piezoelectric effect was first discovered in 1880 by French physicists Jacques and Pierre Curie (the same physicists who suffered premature deaths from their pioneering research on radioactive materials) . The word *piezoelectricity* is derived from the Greek word " piezo" which means to squeeze or press. This effect is found in crystals with no inversion symmetry, which means the crystal structure is non-symmetric. Figure 2 illustrates the piezoelectric effect on the most common piezoelectric material, SiO_2, or quartz. Examples of piezoelectric materials are: quartz, lithium niobate, and interestingly enough, some biological materials such as bones and tendons.

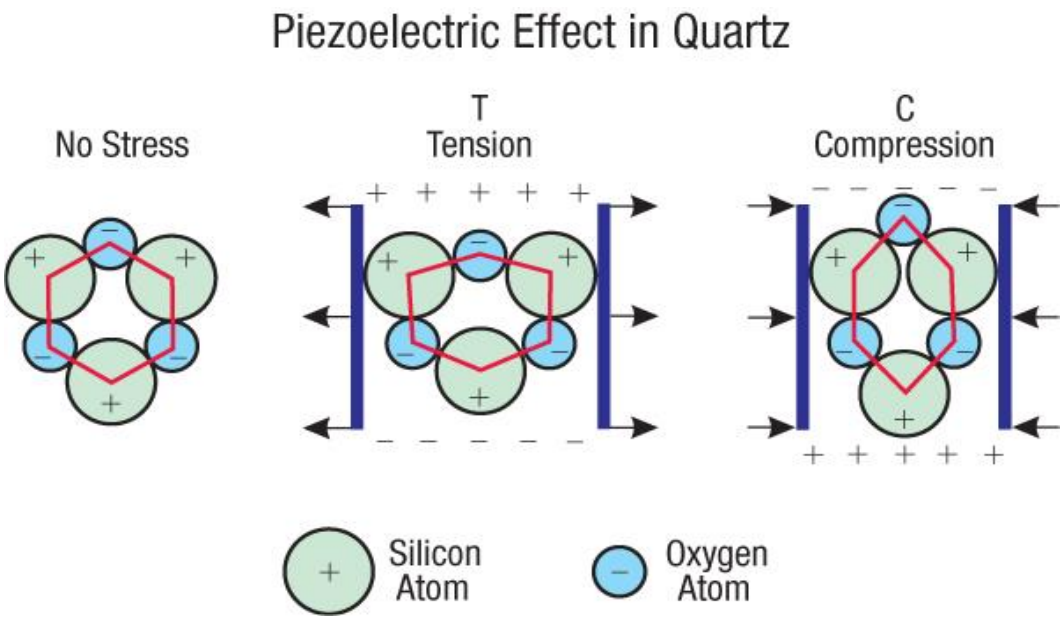

Figure 2- Illustration of the piezoelectric effect in quartz. [2]

The direct piezoelectric effect in a quartz crystal (which is a very common material used in piezoelectric energy harvesting) can be expressed in terms of applied mechanical deformations and an applied electric field. In a simple longitudinal case for linear piezoelectric materials, equation 2 is all that is needed to calculate the polarization. A more general form can be found in equation 5. In the majority of piezoelectric materials, the polarization is directly proportional to the applied electric field (and vice versa, of course). This can be seen in equation 4.

$$(1)\ \sigma \Rightarrow P$$
$$(2)\ P = d\,\sigma$$
$$(3)\ D = \varepsilon_0 E + P$$
$$(4)\ P = \varepsilon_0 \chi_\varepsilon E$$
$$(5)\ P = \sum_{j=1}^{6} \sum_{k=1}^{3} d_{ijk}\sigma_{jk}, \quad \text{(for i = 1,2,3)}$$

The variables in equations 1-5 are defined as follows:

σ	Stress and strain along the crystal axes
P	Electric Polarization
d	Piezoelectic Constant of Material
χ_ε	Electric Susceptibility of Material
E	Electric Field

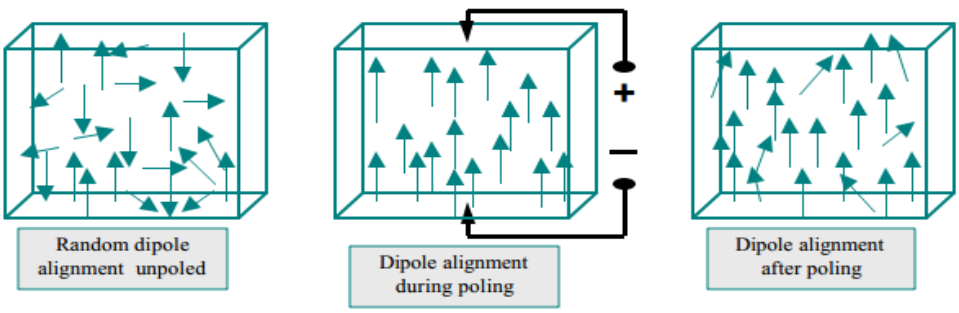

Figure 3- Piezoelectric effect with and without an applied voltage [2].

III. Actuator Selection

After it was decided to move forward with a piezoelectric-based energy harvester, several options were explored before a final decision was made. The criteria used to identify a suitable solution was, first and foremost, power output, but also keeping in mind the mechanical properties, scalability, and price. A thorough electromechanical study that compared several market-available actuators was a good starting point. The parts evaluated can be seen below in figures 4-6, and several observations and conclusions can be deduced from this information.

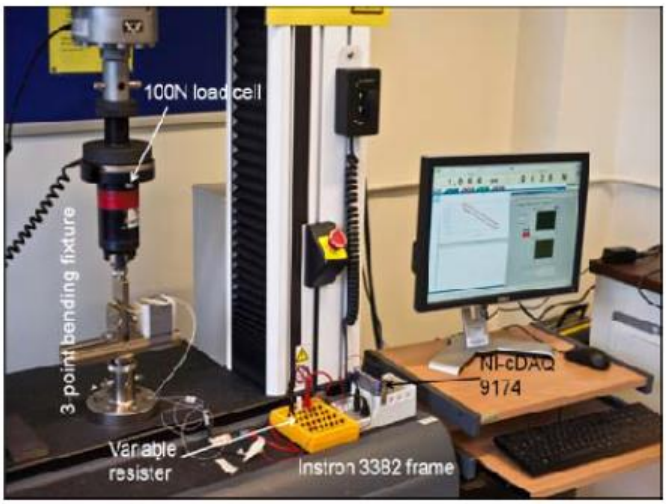

Figure 4- Test setup to evaluate off-the-shelf components [7]

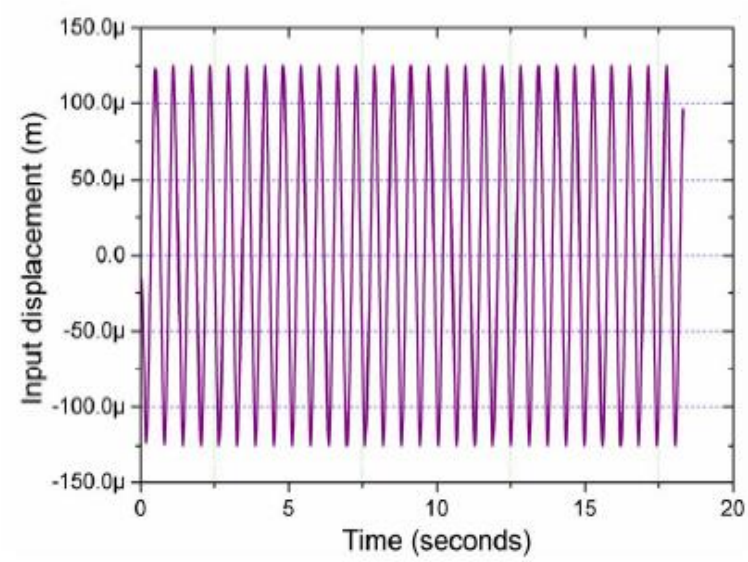

Figure 5- Input displacement for the harvester comparison [7]

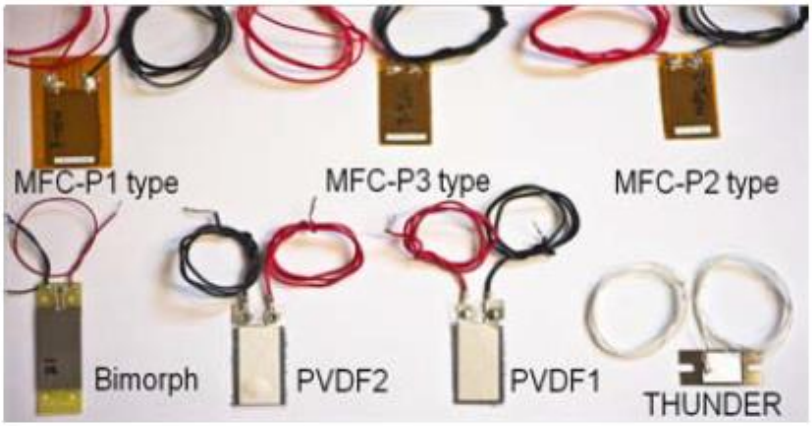

Devices	Active length (mm)	Active width (mm)	Thickness (mm) approx.	Overall length (mm)	Overall width (mm)	d_{33} (pC/N)	d_{31} (pC/N)	Capacitance (nF)
THUNDER	12	12	0.2+0.2	25.32	13.72	390	-190	9
MFC (P1)	28	14	0.3+0.2	38	20	400	-170	0.98
MFC (P2)	28	14	0.3+0.2	37	18	400	-170	24
MFC (P3)	28	14	0.3+0.2	36	16	400	-170	29
Bimorph	31.8	12.7	0.2+0.2+0.1	31.8	12.7	390	-190	41
PVDF1	30	12	0.0052+0.2	41	16	-33	23	0.68
PVDF2	30	12	0.0028+0.2	41	16	-33	23	1.2

Figure 6- The devices tested and their attributes. [7]

The output voltage and power are shown in figure 7. The bimorph device had the highest voltage and power (11V, 55 microwatts) due to the higher volume fraction of piezoelectric material since it used 2 layers instead of 1. The bimorph device also has a higher stiffness (requires more force to displace it a given distance as compared to the others) due to this fabrication. The minimum voltages and power (0.1 V, 5 nanowatts) belonged to the PVDF devices due to the unimorph design and lower stiffness. The THUNDER device, which is known for higher output due to a unique fabrication process [8], was lower than the MFC's due to its low volume fraction of piezoelectric substrate as well as lower dimensions. The MFC's are different due to the difference in piezoelectric modes.

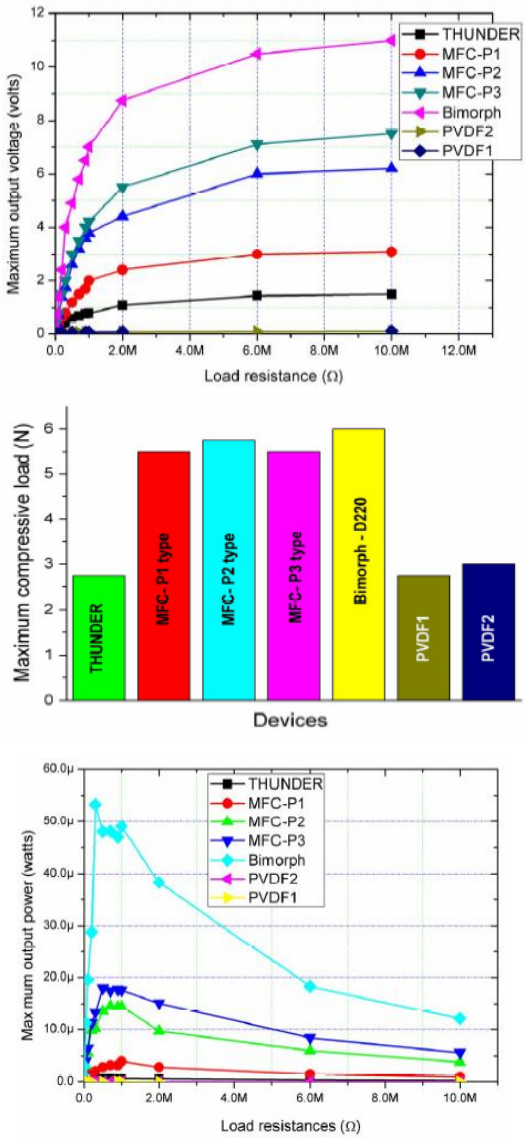

Figure 7- Stiffness and results of the piezoelectric products [7]

It would be easy enough to conclude that the Bimorph actuator would be the one to choose based solely on performance, but several other factors are in play. For one, the Bimorph requires that it be configured in the cantilever configuration, which was not the configuration envisioned in this harvester. Also, the Bimorph was significantly more expensive than the other options. The MFC's (Macro Fiber Composite) from Smart Materials were also explored, and they were a viable option,

but after further investigation it was found that it would need to be mounted to a mechanical fixture in order to operate in the 'simply supported' scheme, which would add to the cost and complexity of the system. In addition, it cost almost double what other devices cost for the same active area. Some attractive features of this MFC are the flexible substrate and available energy conditioning board for a wide range of Vin, but it was determined that, with the advent of a new product from Linear Technologies, this was not needed. The PDVDF actuators were ruled out of consideration due to their poor performance as well as their low availability. It was finally decided to move forward with the Thunder actuators after researching their product line. The Thunder tested in this comparison was actually their smallest model in terms of active area, and their largest offered several advantages over the other actuators including: flexibility, pre-stressed substrate due to unique manufacturing process, lower price point per unit active area, and last but certainly not least, a higher power output when compared to the actuators tested above.

IV. THUNDER Piezoelectric Devices

THUNDER (**TH**in Layer **UN**imorph Ferroelectric **D**riv**ER**) devices are unique piezoelectric actuators that were originally patented by NASA for their space program. The main characteristic of these Thunder devices that sets it apart from the rest of the actuators is its pre-stressed state and unprecedented displacement range.

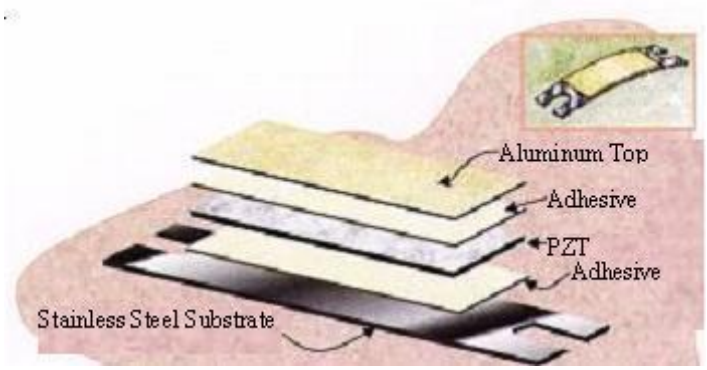

Figure 8- Thunder Construction (Face International)

The Thunder stack consists of a stainless steel substrate, a piezoelectric substrate (PZT 3195HD) sandwiched between two layers of LaRC-Si epoxy, and finally an aluminum plate on top (which is there to act as a shield and to provide a place to solder leads. A specialized manufacturing procedure is responsible for giving the Thunder devices its curvature; a normal piezoelectric ceramic would not be able to handle the degree of stress seen in the Thunder devices. Through many heat and pressure cycles, the device is curved due to the difference in the thermal expansion

and the Young's modulus of elasticity of the stack. Note that the piezoceramic is in a state of compression, while the surrounding layers are in a state of tension.

Figure 9- One of the Thunder 7Rs used in the energy harvester.

The Thunder actuator can be mounted in many different ways depending on the specific application. The two main quantities to consider when choosing a configuration is force and displacement. The most basic configurations are cantilever mounting and simply-supported mounting. It is worth noting that actuators with high displacements tend to output a weaker force, and vice versa. If more force is needed, then these devices can be stacked on top of each other in parallel. If more displacement is needed, then these devices are stacked back-to-back, forming a "clamshell" configuration.

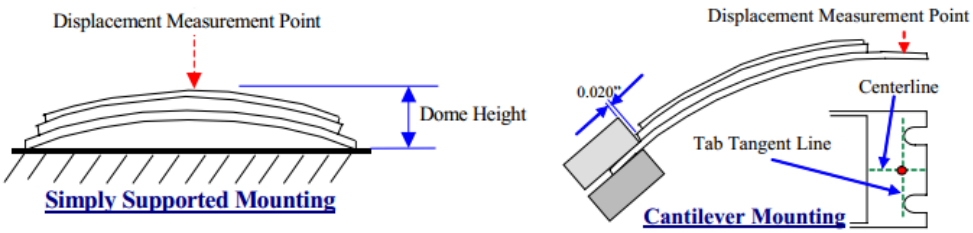

Figure 10- Different mounting options for the Thunder devices (Face International)

There are 6 different Thunder models from Face International, and the 7-R was chosen due to it being the part with the largest piezoelectric active area. Plots of the displacement vs. voltage as well as the force vs. displacement provided in the data sheets can be seen below in figure 11. The most impressive feature that can be seen from these plots is the displacement—other actuators would break well before

reaching the levels that the Thunder is capable of, and the harvester will take advantage of this unique characteristic in order to recover energy.

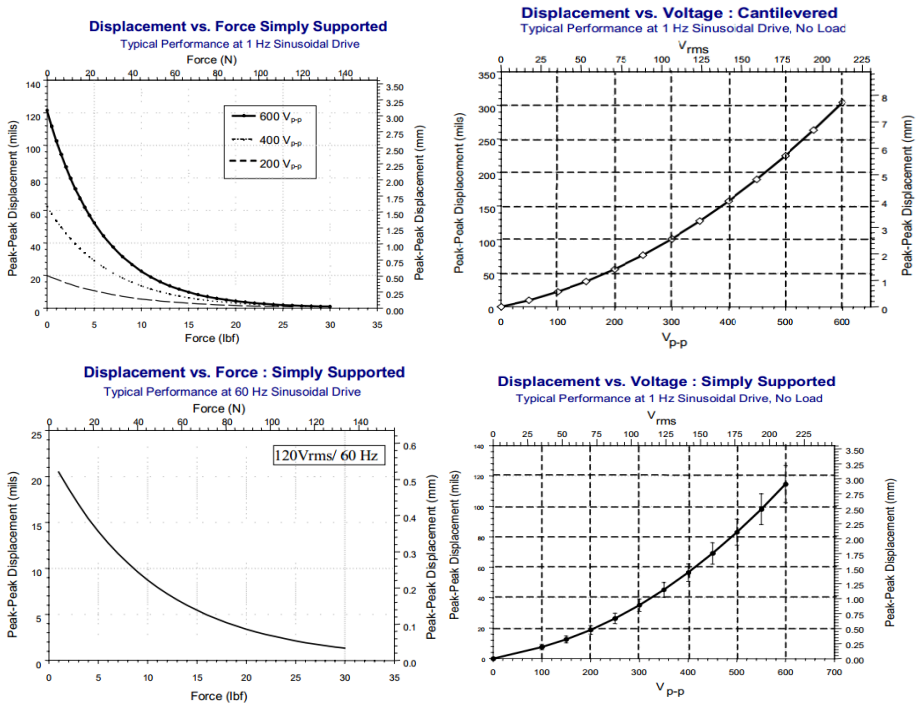

Figure 11- Attributes of the Thunder 7R actuator (Face International)

After contacting Face International, it was discovered that the main limitation in making these devices bigger was the availability of larger PZ substrates from their distributor—at these thickness levels (0.15 mm – 0.38 mm) the substrate is only available at a maximum of 76 x 76 mm. Another reason why it is difficult to produce larger Thunder components is that the difference in stress along the outside edges and the center becomes larger and larger and the substrate size increases, making the assembly unstable or unusable.

THUNDER® SPECIFICATIONS

Model	Weight (gms)	Dimensions L x W x H (inches)	Ceramic Thickness (inches)	Dome/Arch Height[1] (mm)	(in)	Capaci-tance (nF)	Max Applied Volts[2] (Vpp)	Resonant Frequency[3] (c)	(ss)	Typical Cantilevered Displacement[4] (mm)	(in)	Block Force[5] (N)	(lbf)
TH 5-C	2.6	1.25 diam. x 0.019	0.007	1.29	0.051	39	424	NAp	532	NAp	NAp	133	30
TH 6-R	16.3	3.00 x 2.00 x 0.031	0.015	4.24	0.167	77	905	60	NA	3.12	0.123	>133	>30
TH 7-R	18.0	3.80 x 2.80 x 0.023	0.010	9.57	0.377	166	595	31	106	7.62	0.300	133	30
TH 8-R	2.1	2.50 x 0.50 x 0.019	0.008	3.83	0.151	30	480	65	177	1.98	0.078	67	15
TH 9-R	1.0	0.88 x 0.38 x 0.021	0.008	0.61	0.024	7	480	3479	NA	0.12	0.005	31	7
TH 10-R	1.0	1.00 x 0.50 x 0.022	0.008	0.64	0.025	10	480	2854	NA	0.20	0.008	36	8
TH 11-R[6]	0.9	3.00 x 0.10 x 0.029	0.015	NA	NA	4	905	NA	NA	1.98	0.078	NA	NA
TH 12-R[6]	19.5	3.80 x 2.80 x 0.022	0.010	5.49	0.216	139	600	NA	NA	NA	NA	NA	NA

Table 3- The characteristics of the Thunder Actuator Family (Face International)

The maximum theoretical power generated in the Thunder 7R at a given frequency can be calculated by using simple AC analysis. Away from the resonant frequency, the 7R can be drawn in terms of its equivalent circuit that consists of a resistor and capacitor attached to a voltage source. Here it is assumed that the actuator consumes as much power as it produces at a given frequency, which means that it is a reciprocal device. There are small hysteresis effects that can be more or less ignored, for it was found that the calculated power output agrees with the measured power output.

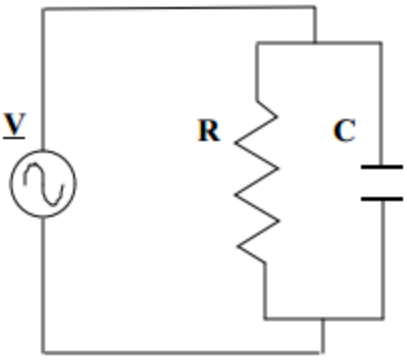

Figure 12- The equivalent circuit of a piezoelectric energy harvester. [4]

$$P_{consumed} = \frac{V_{rms}^2}{R}$$

$$R = \frac{X_c}{tg\varphi} = \frac{1}{2\pi f C tg\varphi}$$

The $tg\varphi$ term represents the dielectric loss and is very small. Thus, a fairly accurate approximation of the power consumed in this device can be realized by finding the reactive power of the device under various excitation stimuli:

$$P_{consumed} = \frac{V_{rms}^2}{R} = 2\pi V_{rms}^2 f C tg\varphi \cong 2\pi V_{rms}^2 f C$$

V. Cookie Wireless Sensor Network Platform

Figure 13- Cookie Node layers. From right to left- processing layer, sensor layer, communications layer (Politécnica de Madrid CEI)

The platform that was used in this project is called the Cookie platform, and this was developed here at UPM primarily by Jorge Portilla back in 2006. The most defining feature of these devices is it's modularity—the platform consists of 4 separate, stackable printed circuit boards, each with its own function. The vertical adapters contained on each layer provide electrical as well as mechanical connections between all the boards. These boards consist of:

- *Power Supply Layer*- Just as the name suggests, this board is used to provide conditioned power to the other layers and is responsible for creating both 3.3 and 1.2 VDC for the microprocessor and communication layers, respectively. This layer can be powered by various sources, such as batteries, USB cables, and/or a supercapacitor (which was used in this case).
- *Processing Layer*- This layer can be thought of as the 'brain' of the node, and it includes a microprocessor as well as an FPGA (if needed for the specific application- some models do not include this to save power).
- *Communications Layer*- The communications layer contains the hardware to send and receive wireless information and relay that back to the microprocessing module. This is traditionally the most power-hungry portion of a WSN node, and much care is taken to assure the power consumption is minimized. There exists two separate 'flavors' of communication modules used in the Cookies- Zigbee and Bluetooth. Both

are low-power communication schemes, and in general ZigBee can support more nodes (over 65,000), uses less power, and has much more flexibility as far as network topology and reconfiguration goes.

Standard	Bluetooth	UWB	ZigBee	Wi-Fi
IEEE spec.	802.15.1	802.15.3a *	802.15.4	802.11a/b/g
Frequency band	2.4 GHz	3.1-10.6 GHz	868/915 MHz; 2.4 GHz	2.4 GHz; 5 GHz
Max signal rate	1 Mb/s	110 Mb/s	250 Kb/s	54 Mb/s
Nominal range	10 m	10 m	10 - 100 m	100 m
Nominal TX power	0 - 10 dBm	-41.3 dBm/MHz	(-25) - 0 dBm	15 - 20 dBm
Number of RF channels	79	(1-15)	1/10; 16	14 (2.4 GHz)
Channel bandwidth	1 MHz	500 MHz - 7.5 GHz	0.3/0.6 MHz; 2 MHz	22 MHz
Modulation type	GFSK	BPSK, QPSK	BPSK (+ ASK), O-QPSK	BPSK, QPSK COFDM, CCK, M-QAM
Spreading	FHSS	DS-UWB, MB-OFDM	DSSS	DSSS, CCK, OFDM
Coexistence mechanism	Adaptive freq. hopping	Adaptive freq. hopping	Dynamic freq. selection	Dynamic freq. selection, transmit power control (802.11h)
Basic cell	Piconet	Piconet	Star	BSS
Extension of the basic cell	Scatternet	Peer-to-peer	Cluster tree, Mesh	ESS
Max number of cell nodes	8	8	> 65000	2007
Encryption	E0 stream cipher	AES block cipher (CTR, counter mode)	AES block cipher (CTR, counter mode)	RC4 stream cipher (WEP), AES block cipher
Authentication	Shared secret	CBC-MAC (CCM)	CBC-MAC (ext. of CCM)	WPA2 (802.11i)
Data protection	16-bit CRC	32-bit CRC	16-bit CRC	32-bit CRC

* Unapproved draft.
• Acronyms: ASK (amplitude shift keying), GFSK (Gaussian frequency SK), BPSK/QPSK (binary/quardrature phase SK), O-QPSK (offset-QPSK), OFDM (orthogonal frequency division multiplexing), COFDM (coded OFDM), MB-OFDM (multiband OFDM), M-QAM (M-ary quadrature amplitude modulation), CCK (complementary code keying), FHSS/DSSS (frequency hopping/direct sequence spread spectrum), BSS/ESS (basic/extended service set), AES (advanced encryption standard), WEP (wired equivalent privacy), WPA (Wi-Fi protected access), CBC-MAC (cipher block chaining message authentication code), CCM (CTR with CBC-MAC), CRC (cyclic redundancy check).

Table 4- Comparison of wireless communication protocols [14]

- *Sensor Layer*- All of the relevant environmental sensors are contained on this board, as well as the appropriate conditioning circuitry for each individual sensor. The sensor information is sent back to the microprocessor element.

Various Sensors Available for the Sensor Board	
-Air Temperature	-Water Temperature
-Accelerometer	-Light Sensor
-Strain Gauge	-Video Camera
-Gas Concentration (CO, NO_2,CO_2, SO_2)	

Table 5- Sensors Available for the Cookie Platform

Design

After identifying the Thunder 7R actuators as the components to be used in this harvester configuration, the design stage commenced. The first step was to envision exactly where this harvester would be used, how it could be installed, and how it would blend into the environment. A system block diagram can be seen in figure 14 and provides a framework to start breaking down the design of the electromechanical system.

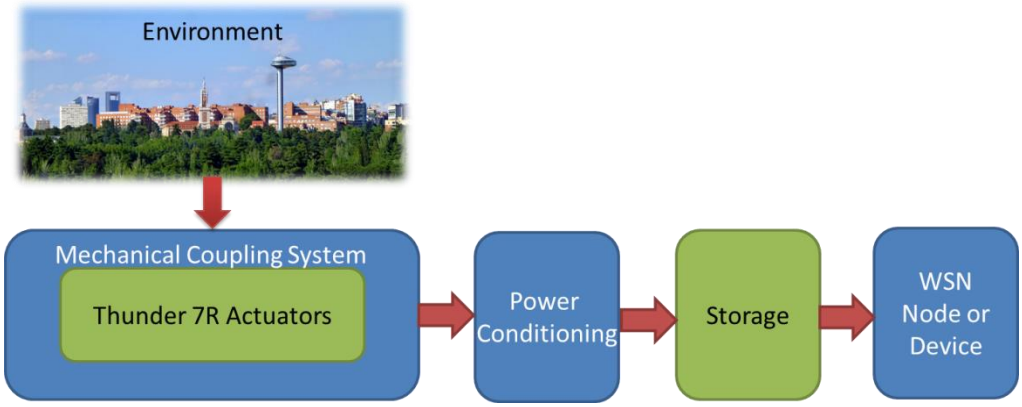

Figure 14- A block diagram for the energy harvesting system

In order to be a truly effective design, this 'black box' needed to be scalable as well as able to be easily adapted to a myriad of indoor configurations. A very expensive and labor-intensive install would be deleterious to convincing businesses and governments to try out this new technology. This box would also have to be as un-evasive as possible; any kind of additional obstacle in the path of the pedestrian to their destination would make their trip longer as well as pose a safety risk. Yet another point to keep in mind was the action of this box when it's stepped on—there would have to be a compromise between maximum power extracted and impact to a pedestrian's step. If the latter were ignored, this box would consist of very potent springs with high spring constants so that as much energy as possible can be recovered due to the oscillating springs pushing the 7R elements up and down.

However, it can be clearly envisioned that this would not be ideal for a city environment.

In order to be a truly effective design, this 'black box' needed to be scalable as well as able to be easily adapted to a myriad of indoor configurations. A very expensive and labor-intensive install would be deleterious to convincing businesses and governments to try out this new technology. This box would also have to be as un-evasive as possible; any kind of additional obstacle in the path of the pedestrian to their destination would make their trip longer as well as pose a safety risk. Yet another point to keep in mind was the action of this box when it's stepped on—there would have to be a compromise between maximum power extracted and impact to a pedestrian's step. If the latter were ignored, this box would consist of very potent springs with high spring constants so that as much energy as possible can be recovered due to the oscillating springs pushing the 7R elements up and down. However, it can be clearly envisioned that this would not be ideal for a city environment.

I. Mechanical

With this in mind, the mechanical portion of the design started to take shape. An aluminum lidded case was taken off a dusty shelf in the lab and proved to be a suitable enclosure for the harvester. The dimensions of this box are 40 x 31 x 9 cm, with the lid being the same height and width but with a height of 2 cm, making the total height 11cm when the lid is placed on top. The lid weighs 2.3 kg, and the bottom half of the case weighs 6 kg.

Next, the springs had to be selected. After some experimentation, it was decided to use 4 springs at each of the corners of the box in order to ensure stability and strength while being stepped on. The springs had to be designed with the following constraints—when 70 kg (average weight of Europeans according to BMC Public Health Studies) load was present on the box the top surface should only yield 1 cm, which is the length required to depress the 7R's completely. Any more distance than 1 cm would mean a risk of damage to the actuators. The springs were designed and build at La Casa del Muelles in Madrid, and the dimensions can be seen below in figure 15. The springs are made from Sandvik Springfield (otherwise known as SH) 4.5 mm diameter spring metal wire, which is a highly touted material for springs due to its high tensile strength, high resistance to corrosion and pitting, and exceptional relaxation resistance. The spring constant was calculated to be 900 N/m from the dimensions and material properties with the following equation:

$$k = \frac{Gd^4}{8nD^3}$$

Where G is the modulus of rigidity of load per meter of deflection, d is the wire diameter, n is the number of active coils, and D is the mean coil diameter (the outside diameter minus the wire diameter). The modulus of rigidity for SH material is 2050 MPa, this will decrease as the diameter of the spring material wire is increased. Plugging these values in yields:

$$k = \frac{Gd^4}{8nD^3} \rightarrow k = \frac{2050(0.0045)^4}{8(5)(0.033 - 0.0045)^3} = 908\ N/m$$

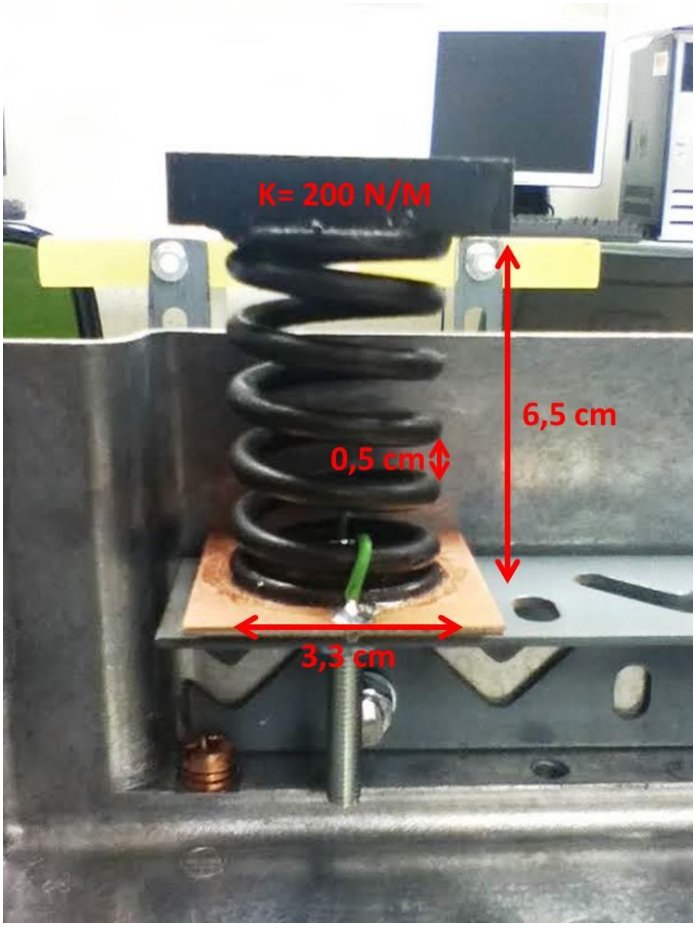

Figure 15- The dimensions of the custom-built springs used in the harvester

It should be noted that with 4 springs supporting the top plate in parallel, the spring constants are additive, making the total spring constant of the system about 3630 N/m. The resonant frequency of mass/spring system with the 6 kg lid is about 24.5 Hz, which is well above the highest anticipated footfall rate. It would be impractical

to increase the lid weight to over 100 kg in order to resonate closer to the expected footfall rate, as this oscillating mass would pose a unique danger to metro passengers.

Now that the enclosure and springs were in hand, they had to be mounted together. This posed a unique challenge in that there were no commercially available mounts for these springs, and a custom-designed mount would cost an exorbitant amount of money. This meant that a home-brewed solution would be needed. After several evolutions the springs were mounted to a PCB square via Loc-Tite super strength glue, and for additional support several strands of enameled copper wire were soldered to the board and weaved through the geometry of the spring. Before attaching the spring to the mount, a size 7 bolt was routed through the center of the PCB so that later it could be bolted to the enclosure. Steel L-sections were then placed around the inner perimeter of the base of the enclosure in order to support the springs.

The simply-supported Thunder devices would have to be mounted on a surface that allows it to slide forward and backwards with minimal interference. It would also have to be a thick insulator as well in order to minimize stray capacitances between the piezoelectric elements and the enclosure. Two identical wooden mounts for the elements were manufactured, and after testing were satisfactory.

The last remaining hurdle in designing the mechanical section was going to be how to effectively push down on the 7Rs without damaging them and maximizing their lifetime. After several evolutions, figure 16 shows the final result. A section of steel L-bar was mounted to the bottom of the lid, which provided a surface to mount the individual arms that would depress the elements. The mounting holes were elongated at both ends in order to provide room to make minor adjustments to the positions of each arm. Attached to the bottom of the arms are pads to make contact with the Thunder devices. The first pad design consisted of a piece of ESD-safe foam attached to a piece of scrap wood, which is in turn attached to another section of L-steel mounted to the arms. This was later changed to filed-down PCB material to act as blades and extract more power from the 7R's. The foam assembly proved to be too sluggish and compressive when pushed down upon, slowing the snap-back action of the actuator, which results in a lower power output.

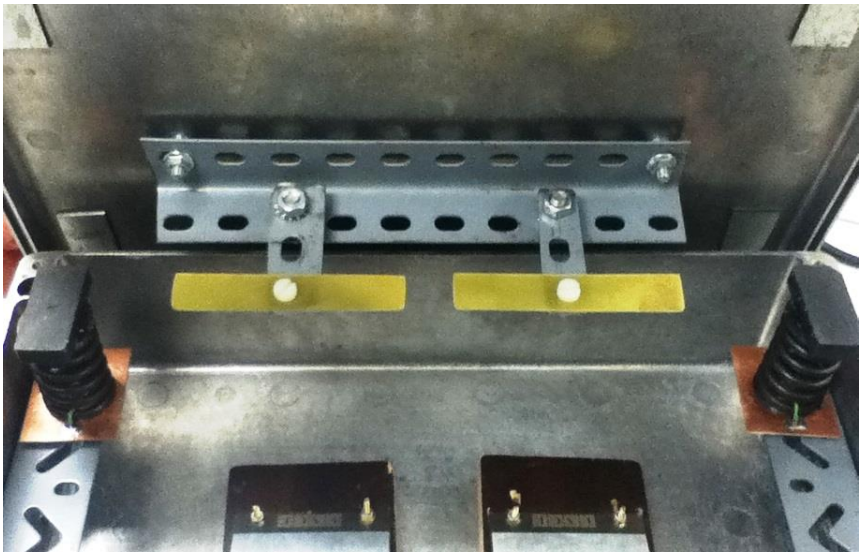

Figure 16- Eventual design of the arms to depress the actuators

Finally, an anti-skid surface was bolted to the top of the box and sunken screws were installed to prevent a pedestrian from tripping. The end result can be seen below.

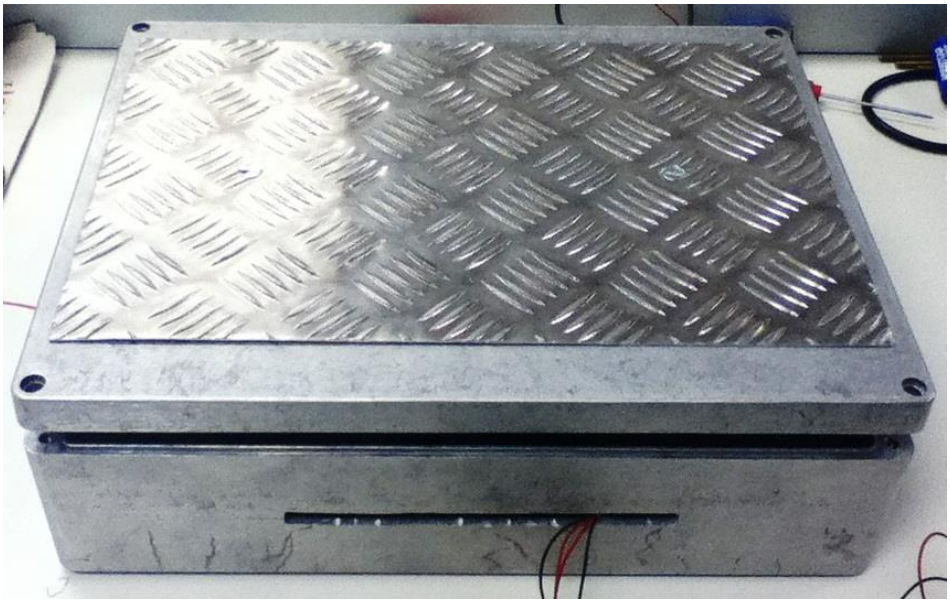

Figure 17- Outer structure of the energy harvester. The slot in the body was installed to route the wires as well as monitor the 7Rs while testing

II. Electrical

The first step in designing the electronics for this project was to characterize the Thunder 7R's in order to get a feel for how these act under varying conditions as well as the ever-important question of exactly how much power can be extracted from them. The devices were mounted to their wooden fixtures and a plastic rod was used to push the device all the way flat. Then the rod was removed from the 7R, allowing it to spring back to its original position. The data was captured using a Tektronix TPS 2024 oscilloscope, and was then imported to an excel workbook that would calculate point-by-point the current from the load resistor value, and then the instantaneous power from the current and voltage. The average power was then found by integrating the instantaneous power using the trapezoidal rule of integration. If this device experiences a footstep once every second (which is a reasonable assumption for heavily trafficked area), then this average power value would directly correspond to the energy produced in joules for every step. After obtaining fairly repeatable results with this method, load conditions were varied in order to find the maximum power output. The results can be seen below in figure 17. From this plot, it can be gleaned that ~150K-270K is the ideal load for maximum power transfer. This same value was witnessed for both of the devices.

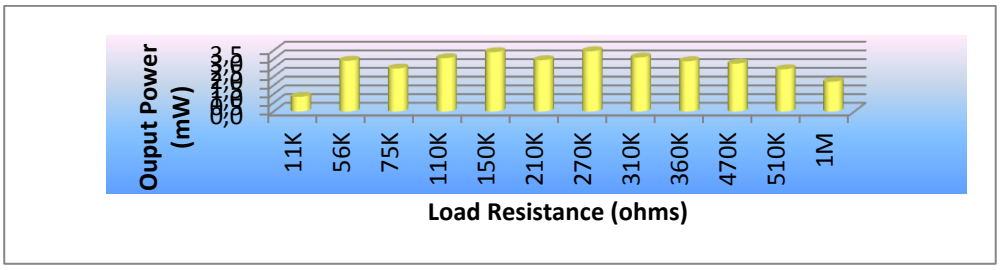

Figure 18- Output power vs. various loads for a Thunder TH7 device experiencing one step

The output for the 150K load condition can be seen in figures 19 and 20. When the actuator is pressed down, a negative voltage develops and peaks to about -60 volts at about 0.42 mA. When the part is snapped back up, the voltage swings positive and achieves a slightly higher peak of about 75 volts at around 0.46 mA . This all lasts for three quarters of a second as the actuator returns to its original arched form.

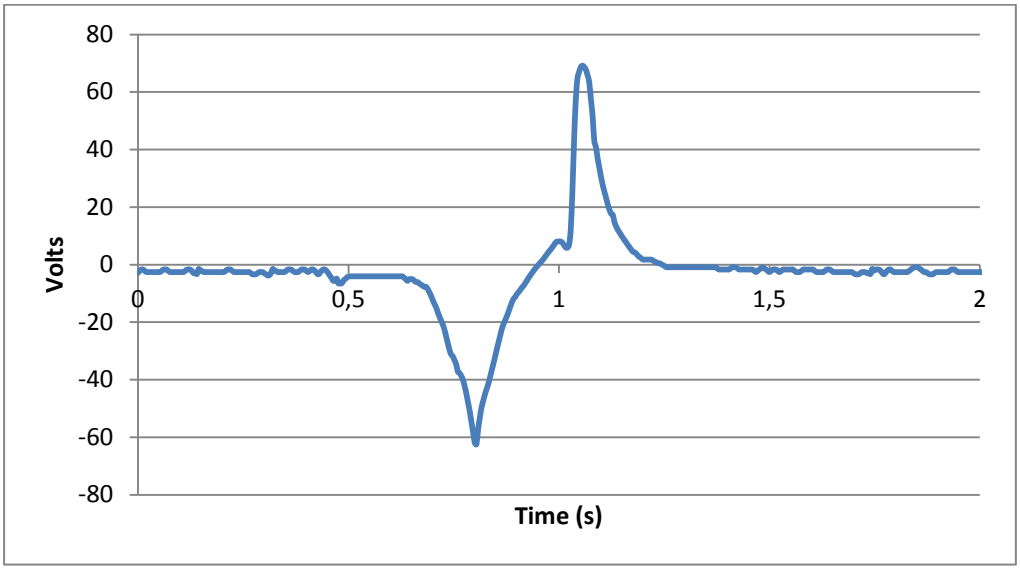

Figure 19- Output Voltage for a Thunder 7R connected to a 150K load after one footstep

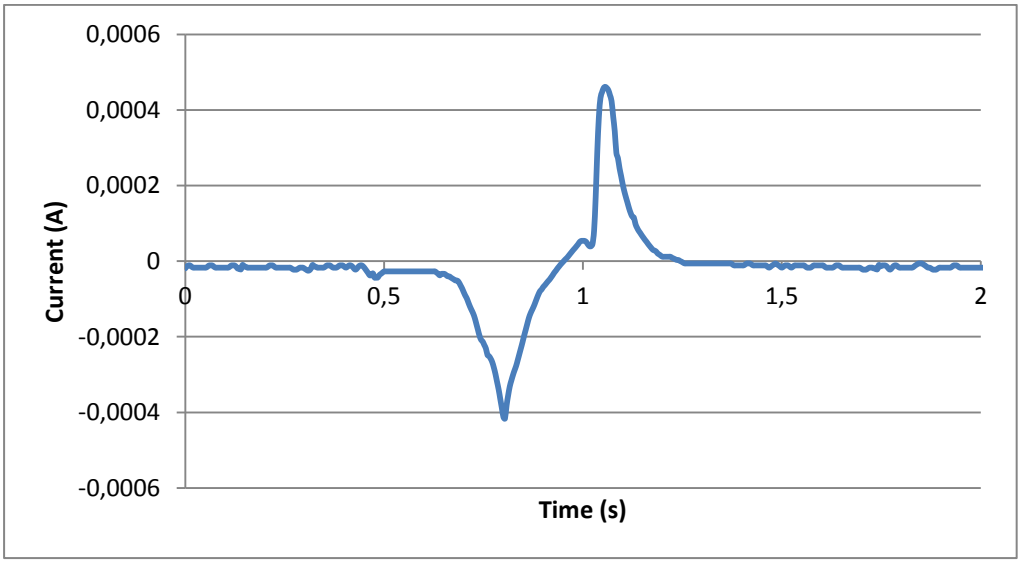

Figure 20- Output current waveform for one step on the actuator with a 150K load

III. LTC3639 Chip

After testing these Thunder 7R's, it became clear that the biggest challenge would be to *efficiently* transform these short pulses of high-voltage, low-current power into something usable. Traditional AC-DC converters made to handle these high voltages are readily available, but after further investigation is was found that the all-in-one regulators are grossly inefficient at the milliwatt power level. Therefore, a new solution had to found or else this project would not provide enough power to justify its utility. Fortunately, Linear Technologies released a new DC/DC converter during the development of this harvester. This modified MSE-16 chip (several pins were omitted to provide some separation between the high voltage pins and ground), the LTC3639, is a high efficiency step-down DC/DC regulator with internal high side synchronous power switches. This converter only draws 12 μA during idle time, which is super important due to the intermittent nature of human traffic—it would be counter-productive if the energy storage was drained rapidly as no activity occurs. The other key factor here is the fact that it can accept a wide range of input voltages (4-150V), and the output is programmable, from 0.8V to V_{in}. These options fall directly in line with the design philosophy that this harvester should be both flexible and scalable. Figure 21 shows the most important plot in the datasheet—the bottom-line, no-nonsense data set of the 3639's efficiency vs. various input voltage levels as well as the current provided to the load at a 5VDC output. The lower bound for acceptable efficiency is around 70%, which corresponds to several different combinations of input voltage and load current.

A general rule of thumb here is to try and aim for load currents greater than 1 mA and input voltages less than 72 V. Previous testing of the Thunder 7R's with a basic full-wave rectifier confirms that this should not be a problem. The operation of this converter can be explained in conjunction with figure 21 below, which provides a block diagram of the chip.

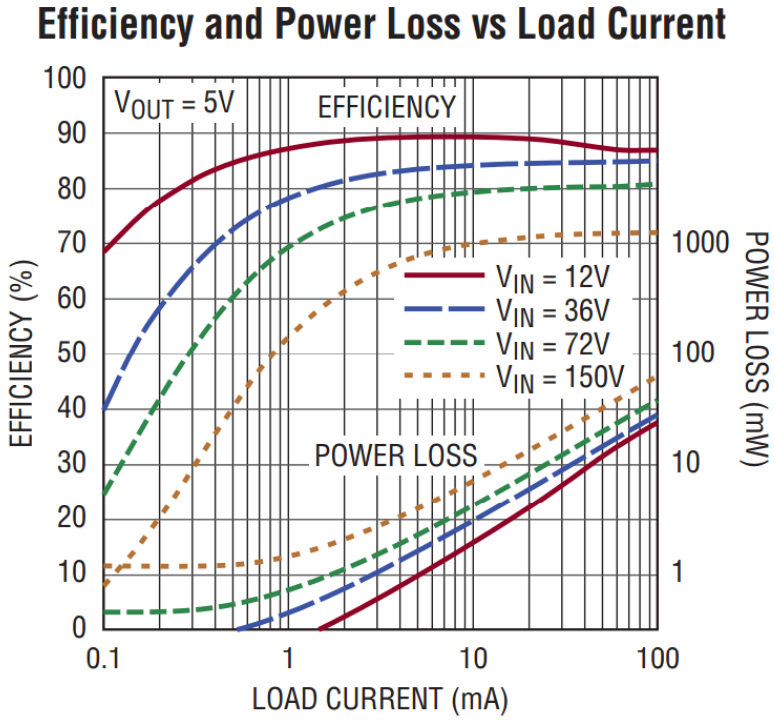

Figure 21- Output efficiencies of the LTC3639 for various input levels (Linear Technologies)

The chip operates so efficiently due to low quiescent current as well as a certain 'Burst Mode' control for the inductor current through the internal power MOSFETs. This 'Burst Mode' can be thought of as a pulse-width modulation scheme, as it controls the amount of burst cycles in a given period based on the current input conditions (see figure 23). For example, under light loads there are fewer burst cycles in a given period that switch on the inductor current, which in turn switch on the power MOSFETs. If there is no Vin, or the voltage on the Run pin falls below 0.7V, the burst circuitry is disabled and the whole chip will go into a sleep mode, drawing only 12 µA. The frequency at which the burst mode operates at depends on the input voltage, output voltage, and the output inductor value. This is hysteresic in nature and inherently provides short circuit protection—the inductor current will decay very slowly during a single switching cycle ($1/f_s$), and the high side MOSFET will not turn on until the inductor current approaches 0.

The output of this chip can be adjusted by either connecting external feedback resistors or configuring the V_{PRG1} and V_{PRG2} pins to connect internal feedback resistors to the V_{FB} pin. Convenient preselected outputs of 1.8, 3.3, and 5V are possible without increasing component count or input supply current.

When powered on, the device constantly monitors the voltage on the V_{FB} pin and compares it to an internal 800 mV reference. If this voltage sinks to more than 5 mV below this reference, burst mode is enabled by the feedback comparator and the part will conduct. If a voltage greater than 800 mV is seen on V_{FB}, the chip disables both the internal switches and the current comparators to enter sleep mode. In this setting, only 12 microamps are consumed.

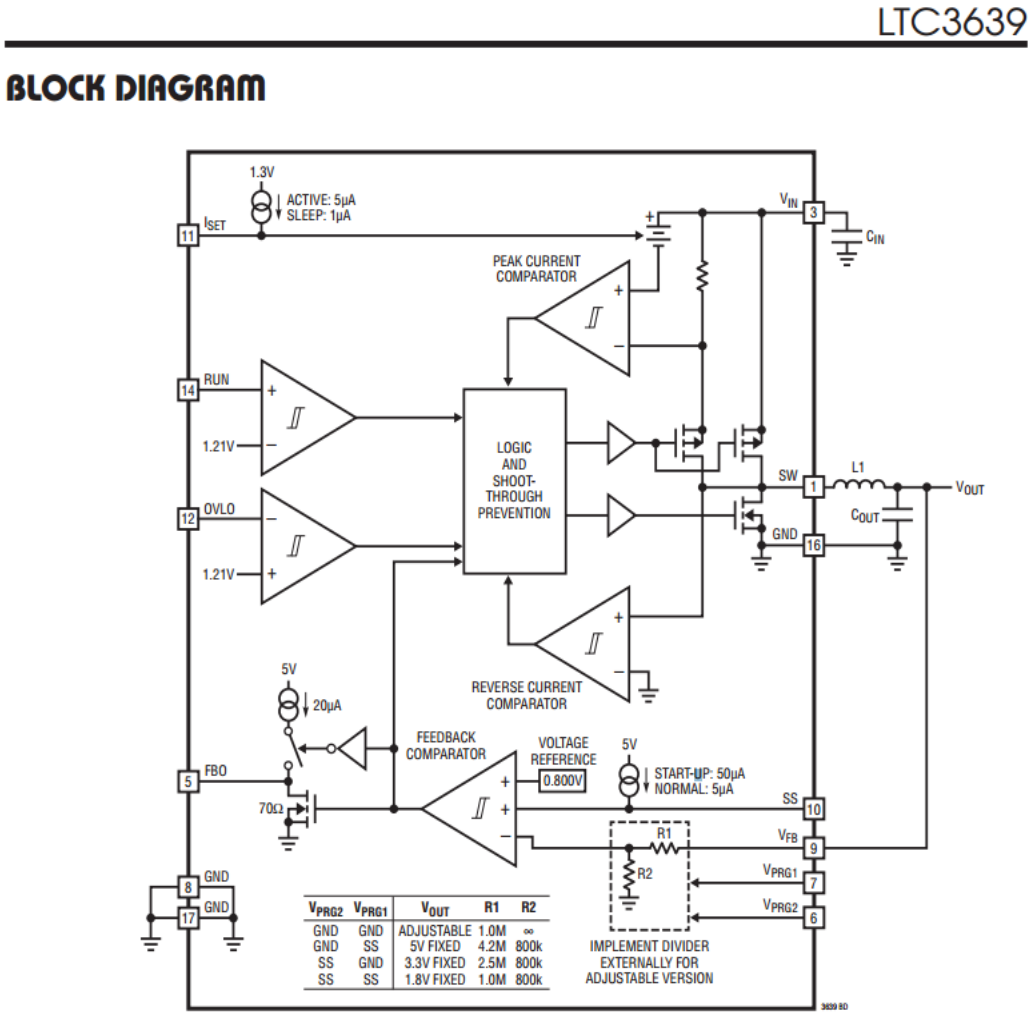

Figure 22- Schematic of the internal circuitry of the LTC3639 (Linear Technologies)

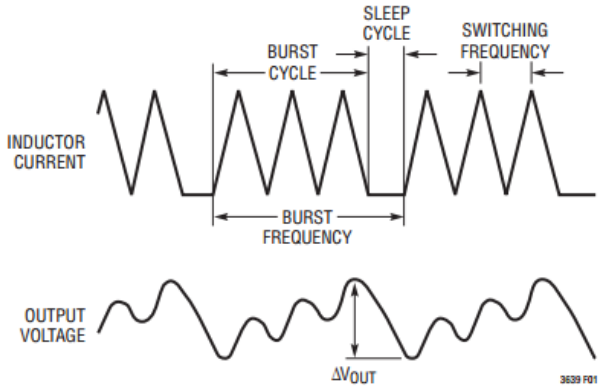

Figure 23- Illustration of the burst mode operation of the LTC3639 (Linear Technologies)

In addition to the lockout conditions outlined above, this component will enter sleep mode if the voltage on the RUN pin falls below 0.7V (and will resume running when this voltage exceeds 1.21V). When the LTC3639 wakes up from a sleep state the internal high-side MOSFET is enabled, causing the inductor current to being ramping up. This will continue until either the inductor current exceeds the value set in the peak current comparator or if the voltage on the V_{FB} pin falls below 795 mV. Note that the peak current value can be set by connecting a resistor between the I_{set} pin and ground. If this pin is left open then a maximum peak current 230 mA is set, and conversely if I_{set} is connected to ground then a minimum peak current of 25 mA would be used.

This component also has several lockout protection features to prevent damage from input transients. Switching is disabled if the OVLO pin rises above 1.21 V, or if the internal undervoltage detector trips when the input voltage falls below 3.5V. The LTC3639 will then recover from these interruptions using a soft-start reset. The reset time is determined by the value of a capacitor from the SS pin to ground, and 1 ms is the default if this pin is left floating.

IV. Component Selection

In order to select the ideal components to use in the power recovery circuit several specifications had to be identified. First and foremost, after testing the 7R's it is known the input range would be about 4-150V. The output voltage will be 5V, as this voltage is very useful for a wide variety of applications. As stated above, the 5V output can be enabled without increasing component count by setting jumpers to the various pins. Table 5 below shows the configuration of the pins for the three separate preprogrammed voltages. Since the Cookie node runs at 3.3 VDC (with a 5 VDC

input being fed to a regulator), it will be of interest to test power consumption with the normal 5 VDC output connected to the node and then the 3.3 VDC, bypassing the input regulator circuit. According to the device specifications, the 3.3 VDC output configuration is inherently less efficient than higher output settings by at least 10%. The peak current should be at least 2 times what the output current is expected to be, and in this case the minimum of 20 mA is more than enough as only 5 to 10 mA are expected out of these 2 parallel Thunder devices. As stated above, this level is set by connecting the I_{set} pin to ground. Now that these basic parameters have been identified, the output inductor can be chosen by using this following equation:

$$L = \left(\frac{V_{out}}{f * I_{peak}}\right)\left(1 - \frac{V_{out}}{V_{in}}\right) \rightarrow \left(\frac{5V}{50kHz * 20mA}\right)\left(1 - \frac{5}{100}\right) = 2.3\ mH$$

VPRG1	VPRG2	Output
GND	GND	Set by resistor divider network
SS	GND	5VDC
GND	SS	3.3VDC
SS	SS	1.8VDC

Table 5- Routing configuration for the preprogrammed voltage output levels

It is also important to note that there exist a couple other constraints for the value of this output inductor. In order to keep the inductor's current well-controlled during the minimum 150ns on/off time of the switches, the inductor must be greater than these minimum values:

$$L > \frac{V_{in\ max} t_{on\ min}}{I_{peak}} * 1.2 \rightarrow \frac{100V * 150ns}{20mA} * 1.2 = 0.9mH$$

AND

$$L > \frac{V_{out} * 3.5\mu H}{1V} * 1.2 \rightarrow \frac{5 * 3.5\mu H}{1V} * 1.2 = 20\mu H$$

There will be higher efficiency with a higher value of L (and hence a lower switching frequency), and so the main concern is to find the balancing point between conversion efficiency and DC losses of a higher inductance value—a ferrite core inductor will be used since they have low core losses and are well-suited to high frequency applications, which is the case here. Special attention needs to be paid to

core saturation when using these ferrite core inductors—they collapse when the core saturates when the peak current is reached, which causes an abrupt inductor ripple current increase and can damage the part. Using the equations above, the provided charts below, a list of available inductor values, and simulation, it was decided to use a 4.7 mH inductor from Toko industries.

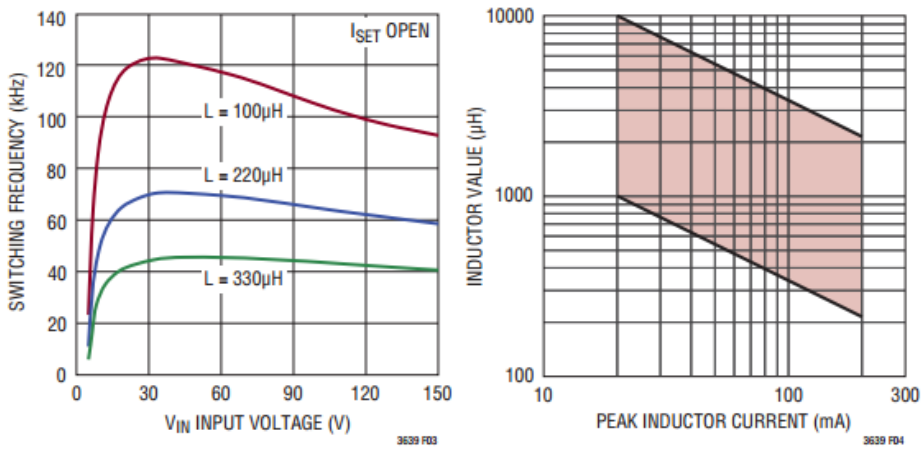

Figure 24- Illustrations on the effect of inductor selection on efficiency and peak current (Linear Technologies)

Next, the capacitors had to be selected. The input capacitor's main purpose is to filter the trapezoidal current that is seen at the top high-side MOSFET's source pin. This capacitor needs to be large enough to provide sufficient energy to magnetize the inductor, while at the same time it needs to keep ΔV_{in} under control and not cause a significant input voltage ripple. With these parameters in mind, the equation used to guide the input capacitor selection is:

$$C_{in} > \frac{LI_{peak}^2}{2V_{in}\Delta V_{in}} \rightarrow \frac{4.7mH * 20mA^2}{2 * 75V * 0.5V} \rightarrow 25nF$$

After looking further into this matter, a 1 µF ceramic capacitor was used since it was easily available and identified as a solid choice for most LTC3639 applications. The output capacitor's main functions are to store the required energy for the load while the LTC3639 is in sleep mode as well as filter the output inductor's ripple current. The output ripple is mainly caused by the feedback comparator's time delay and also it's characteristic 0.5mV hysteresis. To calculate the total output voltage ripple (and then the appropriate output capacitor based on this result), the following relationships are used:

$$\Delta V_{out} \approx \left(\frac{I_{peak}}{2} - I_{load}\right) * \frac{4 * 10^{-6}}{C_{out}} + \frac{V_{out}}{160} \approx 0.03\, V_{pp}$$

$$C_{out} \geq \left(\frac{2 * 10^{-6} I_{peak}}{\Delta V_{out} - \frac{V_{out}}{160}} \right) \geq \left(\frac{2 * 10^{-6} 20mA}{0.03 - \frac{5}{160}} \right) \geq 0.6\mu F$$

V. *Energy Storage*

There are several options available to store this harvested energy, and the exact method is usually specific to the node's application and available harvested power. Lithium-ion batteries have the advantages of being cheap, widely available, and have a high energy storage density, but after many charging and recharging cycles the battery degrades. Also, lithium is not as easily recycled and is a harmful element for the environment.

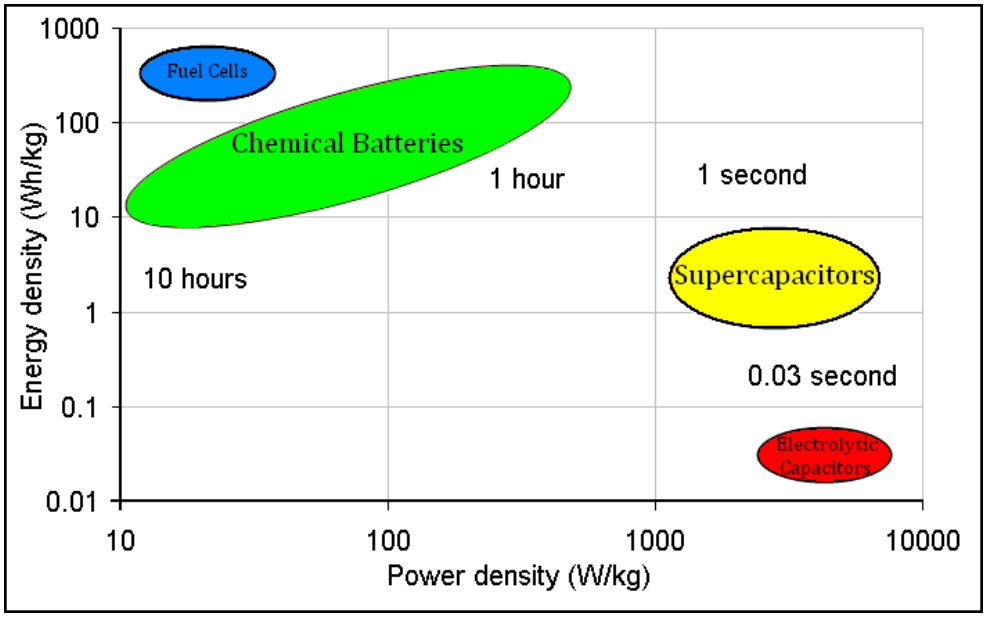

Figure 25- Visualization of energy and charge densities for various storage methods (Maxwell Technologies)

Traditional capacitors are quickly charged/discharged and are not as harmful to the environment, but can only store very limited amounts of energy and have orders of magnitude less energy storage density than lithium-ion batteries. This makes capacitors only suitable for ultra-low power applications where the harvested energy is used almost as soon as it is acquired—the capacitor will begin to discharge quite rapidly. The third option is a supercapacitor, which more or less bridges the wide gap between capacitors and lithium-ion batteries. Supercapacitors come in a variety

of flavors and the term itself is bloated and can refer to ultracapacitors, electric double-layer capacitors, or exotic nano-storage devices. They can offer very quick charge and discharge periods, which is well-suited to WSN applications as the nodes are only activated for very short periods of time. Supercapacitors are widely used as complements to traditional energy sources since they can handle power peaks without compromising their lifetime. They have much lower ESR than traditional capacitors, which means the leakage current is much less. The obvious disadvantage of supercapacitors is that they cannot power a hungry load for an extended period of time, so the designer needs to keep this in mind when developing the node.

Traditional capacitors are constructed with 2 metal plates and a dielectric material separating them. When a voltage is applied, charges populate the plate/dielectric interface. The total capacitance is based on the dielectric material properties, the plate area, and the distance between the two plates. A double layer electrolytic capacitor, such as the one used in this project, is constructed with activated carbon, and an electrolyte separator. Activated carbon is extremely porous and as a result has an extremely high surface area to volume ratio. For example, an eraser-sized piece of activated carbon has roughly the same surface area of a tennis court! This means it is able to hold an incredible amount of electrons when compared to traditional metal-plate based capacitors. Figure 26 below shows the construction and action of the EDLC.

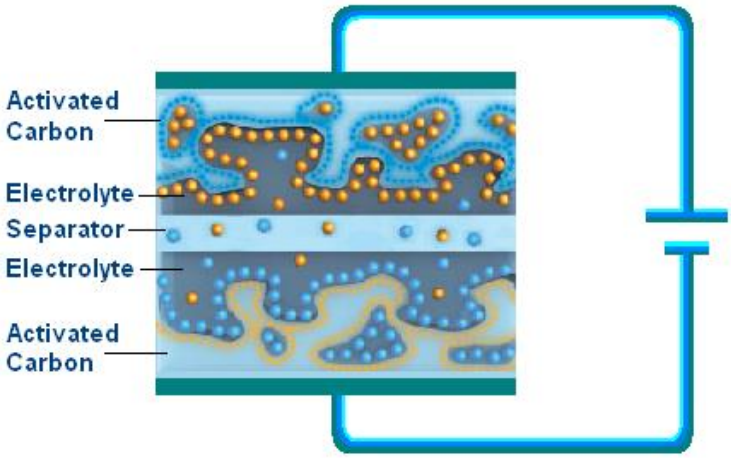

Figure 26- Diagram of an ultracapacitor (Michigan State University Engineering Dept.)

Simulation

After identifying the components to be used in this circuit, a PSPICE model was created in order to confirm the proper operation and to get an idea as to how the most important parameter, the power output, would be affected by adjusting the component values calculated above. The schematic can be seen in figure 27, and in addition to the LTC3639 circuit this simulation consists of two current sources, a fullwave bridge rectifier, and a storage capacitor. The 10 mF storage capacitor was chosen since it was the largest conventional capacitor available in the laboratory and would provide a real-life metric to compare the simulation to. The available supercapacitor (the Maxwell BPAK0058) took far too long to charge for efficient troubleshooting. The two sources represent the Thunder 7R's and were programmed with captured waveform data from the 7R's as well as the equivalent series resistance (set to 200 milliohms to account for the contacts and wiring) and parallel capacitance (166 nF per the manufacturer specifications). The model for the diodes was silicon ES1D's from Vishay International, which were very similar to the diodes used in the full-wave bridge rectifier. The inductor and capacitors' parameters were chosen such that they closely matched the parameters of the real components selected. The LTC3639 model was provided by Linear Technologies.

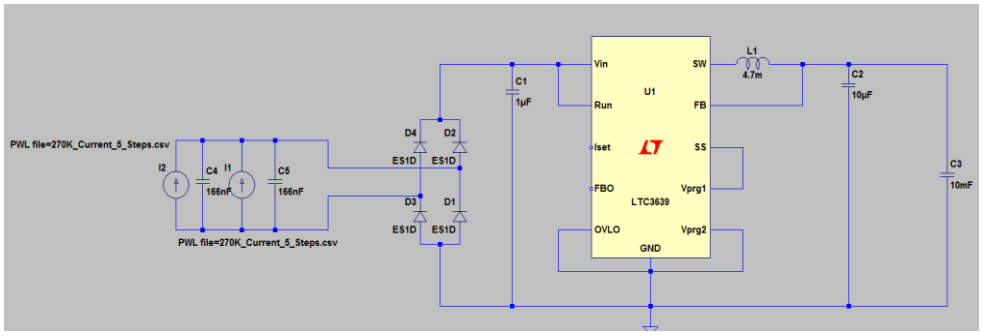

Figure 27- View of the PSICE simulation environment used in this research

After some obligatory tweaking to get the simulation software to behave controllably, the results and final values selected can be seen in the figures below. The input current waveform in figure 28 was captured using an oscilloscope and subsequently programmed into the model of the current sources. The waveform was taken from a person stepping onto the energy harvester one single time. After performing this many times and establishing repeatable results, this waveform was then saved as a CSV file. Using excel, this waveform was cleaned up and then

stitched together to form a train of pulses at 1.5 Hz. This yielded 1.25 mJ in 10 seconds for a single Thunder 7R device.

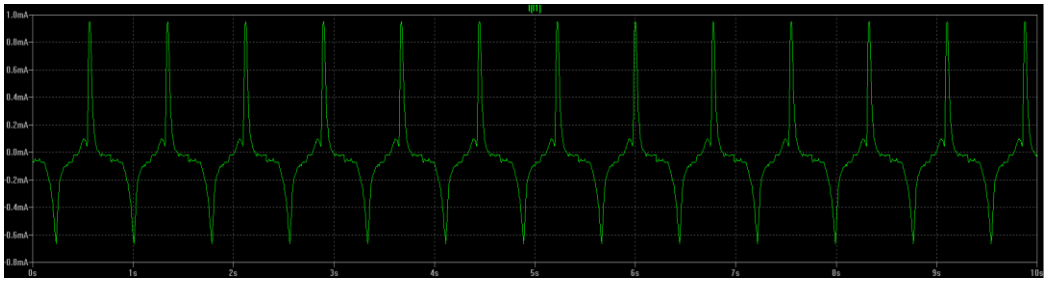

Figure 28- Input current waveform at 1.5 Hz for the current source input

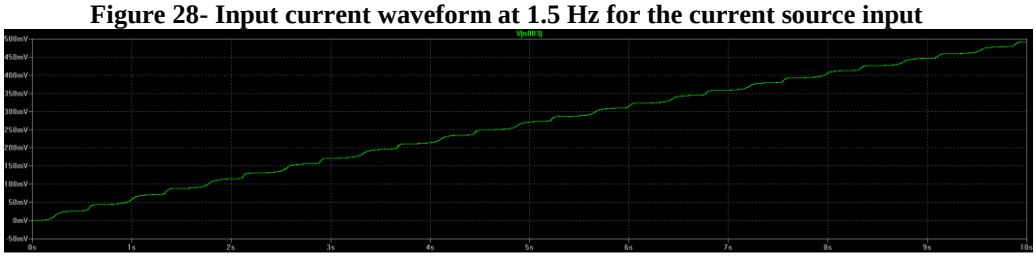

Figure 29- The voltage on C3 with one 7R at 1.5 Hz. In 10 seconds it generates 1.25 mJ at a rate of about 48 mV/s.

The next figure shows the results when either 4 Thunder 7R's are used with the same footfall frequency of 1.5 Hz. This yields about 3.6 mJ in 10 seconds:

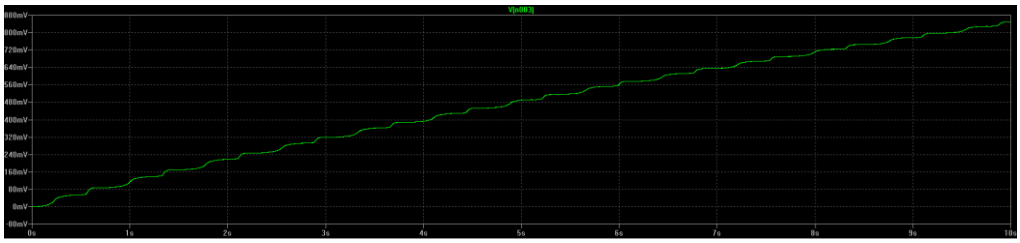

Figure 30- The voltage on C3 with 2 7R's at 1.5 Hz. In 10 seconds it generates 3.6 mJ.

When the Thunder count is increased to 6, the output energy follows suit and increases as well, yielding about 6.6 mJ. This means that depending on the WSN node requirements, the number of actuators can be scaled in order to accommodate the demands of the node's circuitry. As it will be seen later in the construction, testing, and implementation phases, the amount of power generated only tells part of the story—the power requirements will change based on the node's algorithm, the leakage current of the storage element, and of course the footfall pattern of the harvesting zone.

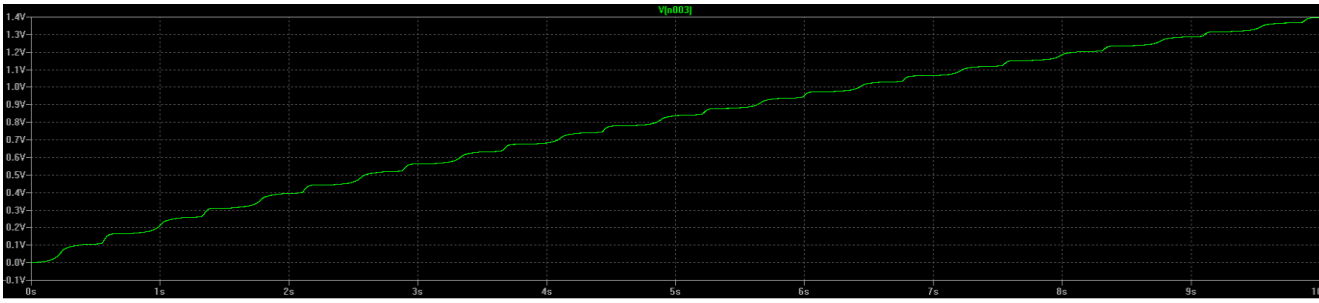

The voltage on C3 with 4 7R's at 1.5 Hz. In 10 seconds it generates 6.6 mJ.

To start to compute the efficiency of this system, a rough calculation of the energy produced in a single footstep should be compared to the energy per footstep produced by a Thunder 7R, which is 1.2 mJ/13 steps, or 92.3 µJ. The energy in a single footstep, assuming a person and their effects weigh 80 kg, and that the enclosure lowers 1 cm when stepped on is:

$$F = ma = 80kg * 9.8\frac{m}{s}$$

$$= 784N\ or \sim 1000N\ (considering\ the\ added\ acceleration\ of\ a\ persons\ foot)$$

$$W = FD = 1000N * 0.01\,m = 10\,J/step$$

$$Efficiency = 92.3\frac{\mu J}{10J} = \ll 1\%\ for\ 1\ 7R\ actuator\ with\ power\ conditioning$$

This is obviously a very disheartening result, and the efficiency was not notably improved even when exploring different output inductor values. However this is not a death sentence, as even these power levels can be enough to enable many applications.

Construction

After simulating and confirming the operation of the circuit, a PCB needed to be designed and constructed for the prototype. Unfortunately a prototyping board was out of the question due to the lack of availability of an adapter for the miniscule MSOP-16 footprint of the LTC3639, and the developer board from Linear Technologies was too pricey and included many options not needed in this application. It took several iterations and redesigns to get this board to develop properly with traditional silk-screening methods due to the very demanding line width specifications, which were 0.5 mm. The board was developed with the Altium software suite, and the final design can be seen in figure 32 below. Unfortunately, a jumper could not be avoided for the connection between the V_{in} and the Run pins. Due to the extremely small tolerances, an inter-chip via could not be achieved with one layer without shorting to the ground plane that the back contact of the chip requires. The board was limited to only a single layer due to the normal PCB etcher machine being out of operation. Per the recommendation of Linear Technologies, a large ground plane was included in order to minimize ground impedance due to the significant current loops between the power switches and C_{in}.

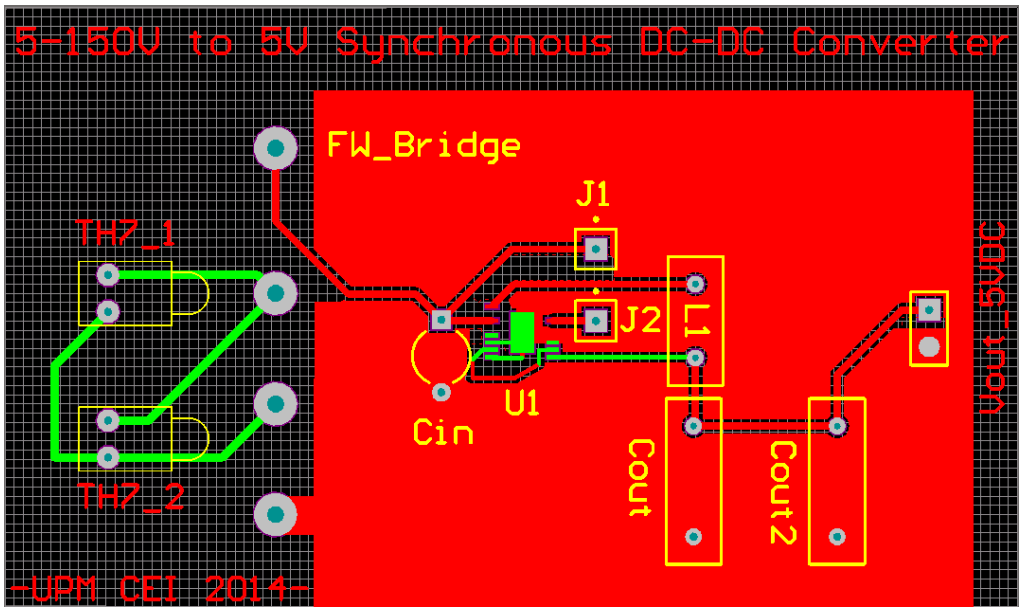

Figure 32- Board design for the power conditioning circuitry using the Altium PCB design suite

In addition, the input capacitor was placed as closely as possible to the V_{in} pins to minimize I^2R loss as the capacitor feeds the switches current. One more consideration was placing the SW node away from any sensitive small signal nodes, as the high frequency switching can couple with high impedance nodes and is detrimental to the output ripple. An additional C_{out} spot was installed in case several had to be used to arrive at a particular value. This single-layer board is 70 mm wide and 87 mm high, which makes it very compact and suitable for even very small harvesters. The finished circuit board can be seen in figures 33 and 34. In addition, the parts list is contained in table 6.

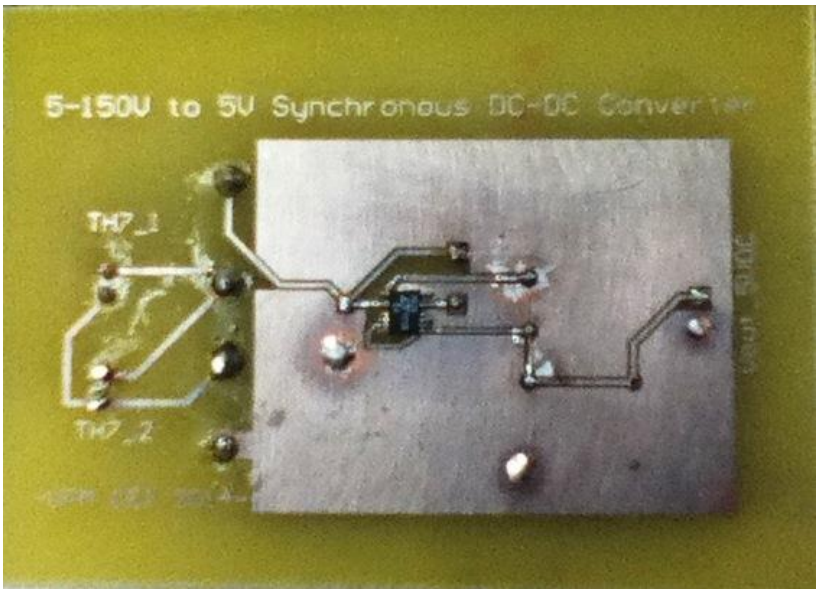

Figure 33- Back side of the PCB after construction

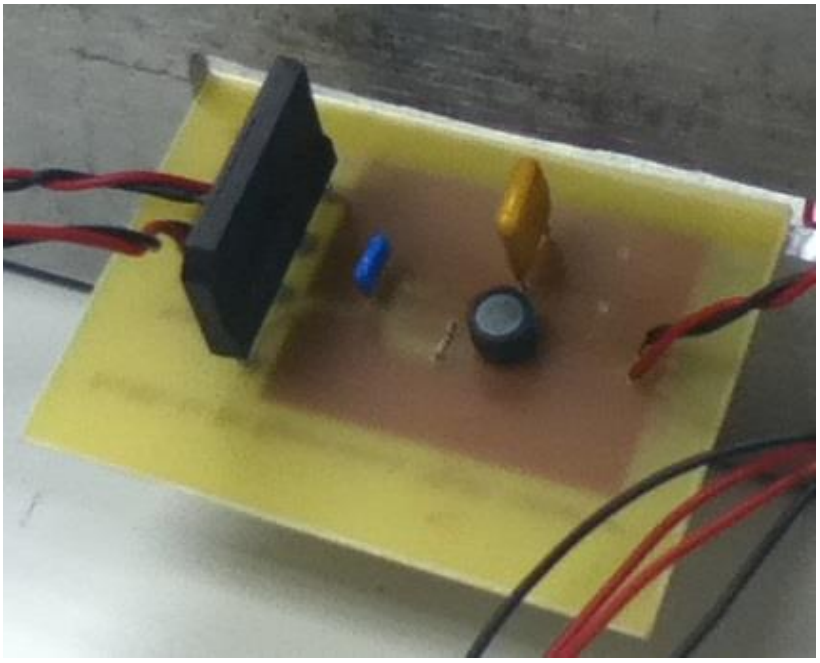

Figure 34- Front side of the PCB after construction

The parts list as well as the total cost can be seen below. The total cost of materials for this prototype harvester was about 250 euros, which would increase if the scrap materials scavenged had to be purchased. The Cookie WSN platform was also donated by the department; it would cost a couple hundred euros to purchase one separately from a supplier. A good estimate for this system would be 600 euros if all the materials had to be purchased new.

Component	Quantity	Unit Price	Total
Aluminum Case and Scrap Metal	1	N/A- Salvaged	€0
Thunder 7R Actuator	2	€100	€200
LTC3639	1	€6	€6
Misc HW/Components	1	€20	€20

Toko Inductor, 4.7 mH 262LY-472K	1	€2	€2
Maxwell 15V, 58F Supercapacitor	1	N/A- Donated	€0
Cookie WSN Node	1	N/A- Donated	€0
Bridge Rectifier, Vishay GSIB620	1	€2	€2
Custom-Made Springs	4	€5	€20
Magnets	4	€0.50	€2
	Total		**€252.00**

Table 6- Parts list and total cost of the piezoelectric energy harvester prototype

Testing

Now that the operation of this circuit is confirmed, several factors need to be identified and understood in order to pair this harvester with a wireless sensor network node (and in this case, the Cookie node). A good starting point is the power consumption profile of the Cookie, since this will determine whether or not a self-sufficient node is possible with the amount of energy harvested. This profile will change drastically depending on the specific application, but for now we are considering a node that is sleeping, wakes up every *x* minutes to take and wirelessly send a sensor reading, and then falls back asleep again. This single event process takes about 4 seconds, with the wake-up and subsequent fall back asleep state transitions taking about 0.5 seconds apiece. The power consumption of an event can be seen in figure 35 below. The Cookie consumes about 2.3 J in one hour of sleeping, and an additional 320 mJ for every node event (wake up, read sensor, send sensor information via ZigBee, go back to sleep). This means that the harvester needs to not only account for this energy, but also leakage from the storage element(s).

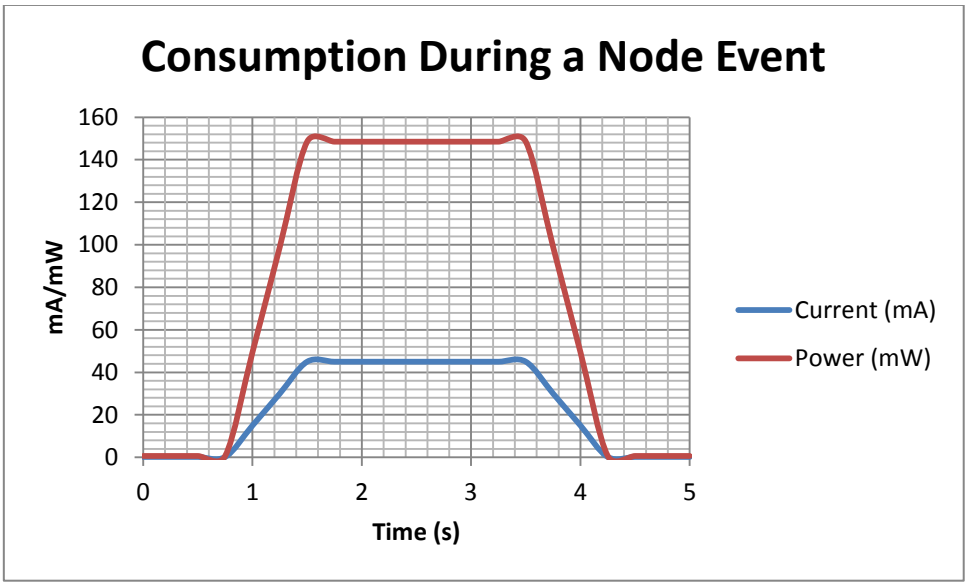

Figure 35- Power and current consumption for a Cookie node event

Of course, the power requirements of the node vary greatly depending on the mode that it is operating in. Looking at figure 36, the energy requirements for one hour of operation is shown as a function of the number of node events in that same hour. As stated before, each node will consume 2.37 joules in one hour for just being in sleep mode, and each event adds 319.5 mJ to the total energy consumed. The impact of the node not being in sleep mode for as long due to many events is negligible compared to the total amount of energy expended to keep this node operational.

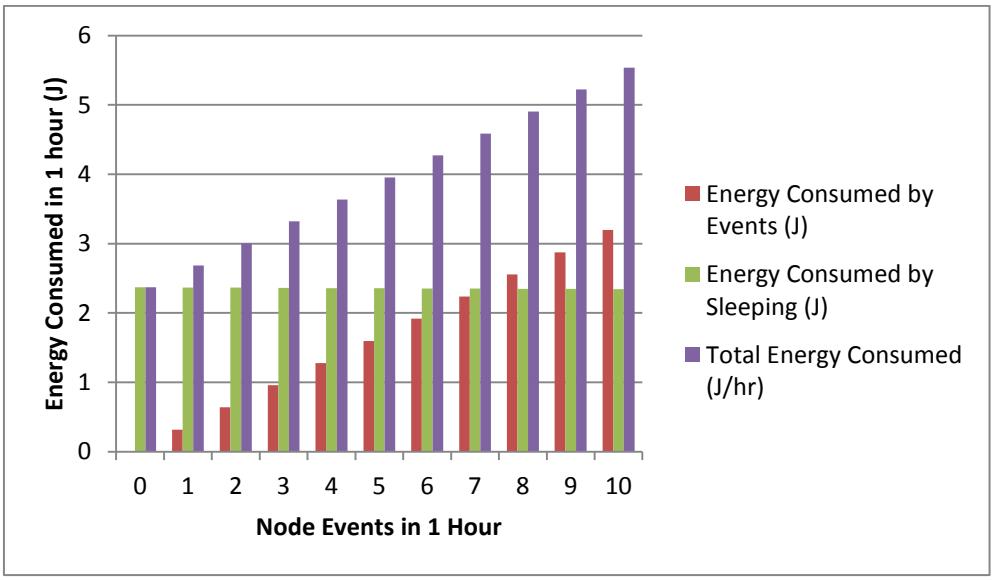

Figure 36- Power Consumption profiles for ascending event counts

Unfortunately, during testing one of the Thunder 7R's was destroyed and another could not be attained before the testing phase was completed. However, testing this one 7R with the harvester would be enough to confirm the validity of the simulation, which could then be used to explore many different configurations. The power conditioning circuit was tested with a single Thunder 7R connected to the LTC3639 circuit and charged a 10 mF, 50 VDC electrolytic capacitor. This value was chosen to see if the charging time and energy levels matched the calculations of the simulation, and also to see exactly what energy levels this harvester is capable of producing. The supercapacitor was not used in this case, as it would take hours and hours of jumping on the harvester to charge it up to a useful voltage.

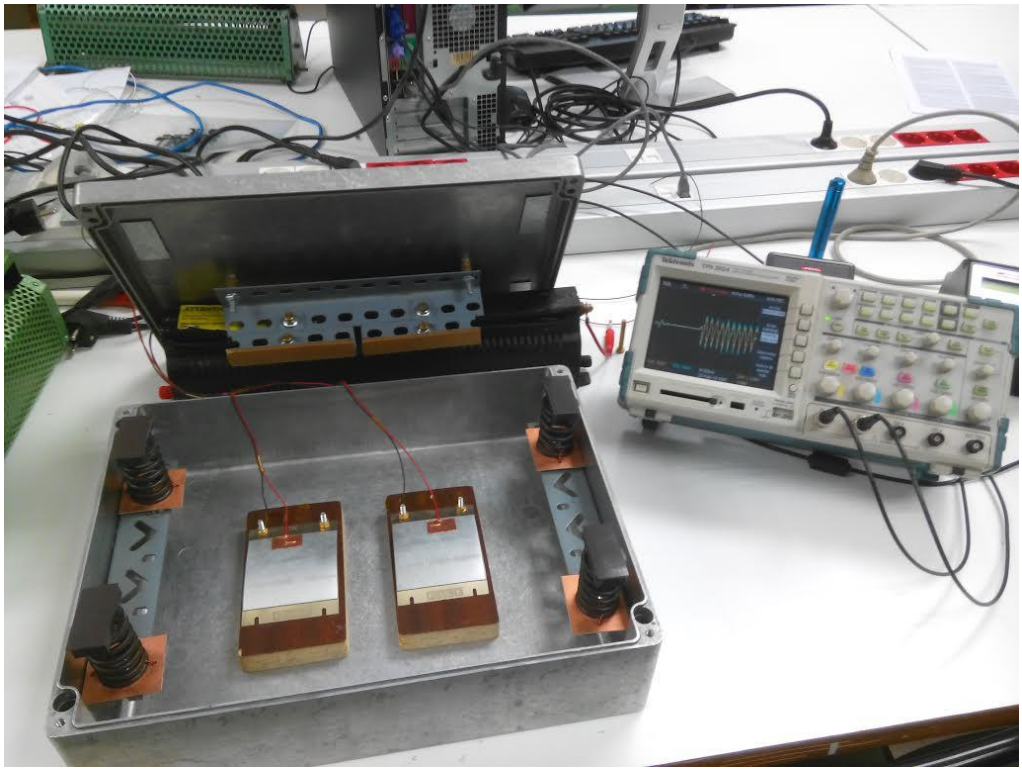

Figure 37- Testing setup for the Thunder 7Rs mounted into the case

The frequency was manually set by monitoring a clock and making sure there were 3 jumps every 2 seconds, which was roughly what can be expected in a busy corridor based on real-life observation in the Sol metro station in Madrid. Figure 38 shows the results of this experiment; with one Thunder 7R the harvester can produce about 11.25 mJ per minute. The charging rate matched relatively closely to the simulation (41 mV/s measured, 48 mV/s simulated). Of course, these capacitors are notoriously leaky (especially with the low power levels being worked with here), and will discharge when not being used. This was measured to be about 1.8 mJ per second, making the net energy output of the harvester with one Thunder 7R decrease very rapidly when there isn't constant traffic. In the final implementation, a supercapacitor will be used to prevent this unnecessary waste of energy—the Maxwell BPA00058 was measured and leaks only about 9.6 mJ per minute, or 0.16mJ per second with no load attached.

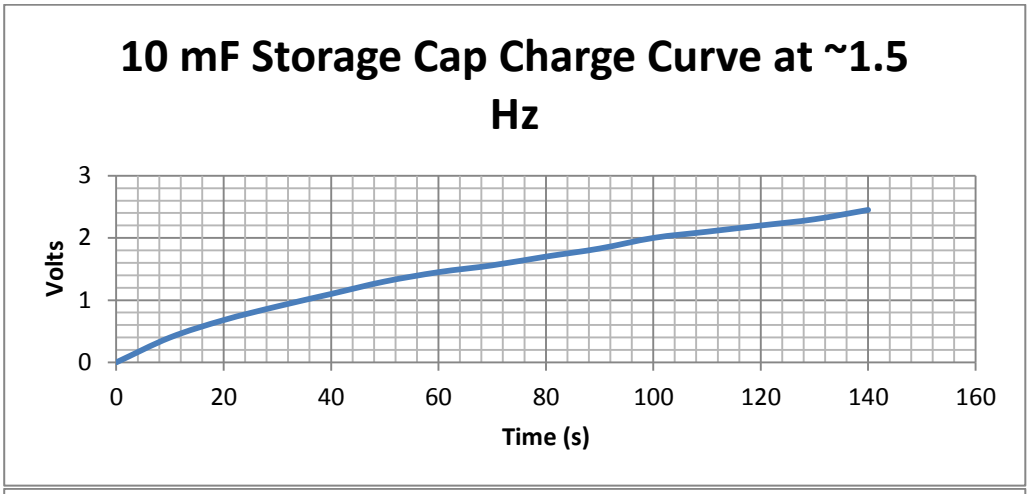

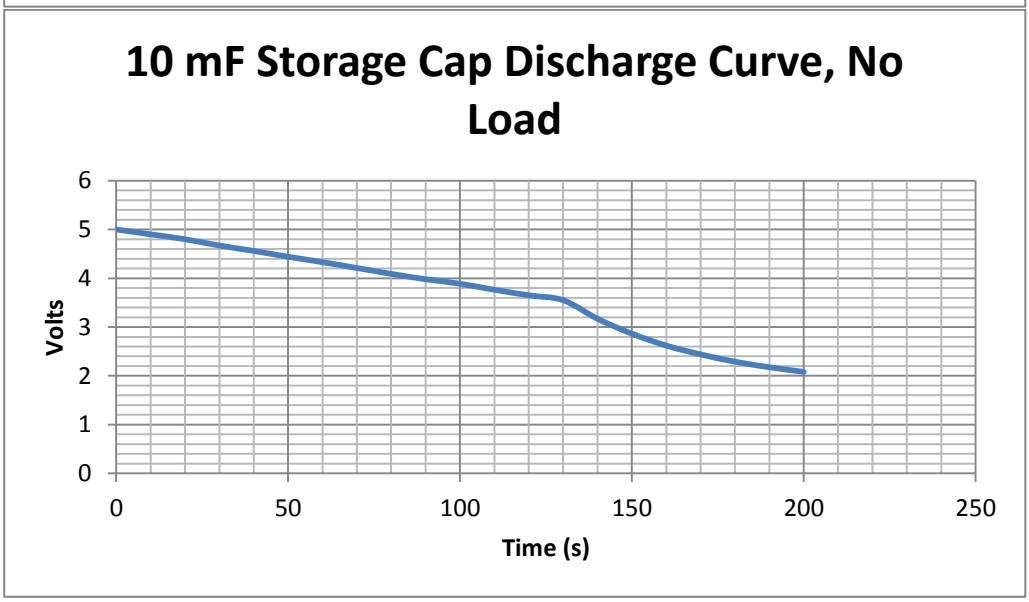

Figure 38- Charge and discharge curves for 10 mH, 50V elecrolytic capacitors

Implementation Example

In this implementation, a Wireless Sensor Network solution will be explored for the bottom of the stairs of the main exit at the Sol metro station in Madrid. In order to save money on heating/air conditioning and to optimize the train schedule, both temperature and footfall measurements are desired at least 4 times per hour. It is of interest to find out the minimum number of Thunder actuators needed to support this node as well as the cost and limitations of implementing this system.

Parameter	Value/Assumption
Footfall Rate **8-10 am, 6-8 pm**	Constant traffic 80% of the time (3 metro lines converge here, arrive every 3.5 minutes at this time)
Footfall Rate **6 -8 am** **10 am – 12 pm** **8pm – 12 am**	Constant Traffic 60% of the time (The 3 metro lines arrive every 5-7 minutes)
Footfall Rate **12pm – 6pm** **12 am- 2 am**	Constant Traffic 50% of the time (The 3 metro lines arrive every 7-9 minutes)

Table 7- Approximated footfall for a workday at the main exit of the Sol metro station

After tabulating this information, a graph was made to visualize the difference in power storage as the 7R actuator count was increased. These tabulations took into account the discharge of the capacitor (34.4 J/hr for the supercapacitor), and the expression used was:

$$E_{mJ/hr} = 640mJ * r_{footfall} * n,$$

where 640 mJ is the amount of measured energy that the harvester with one Thunder 7R can produce in 1 hour under 1.5 Hz excitation, $r_{footfall}$ is the footfall rate, and n is the amount of Thunder actuators used in the assembly. The total amount of stored energy was calculated by summing up the amount of energy produced hour-by-hour. The results are not surprising, and will form a baseline for figuring out how many actuators would be needed for x amount of node events per hour.

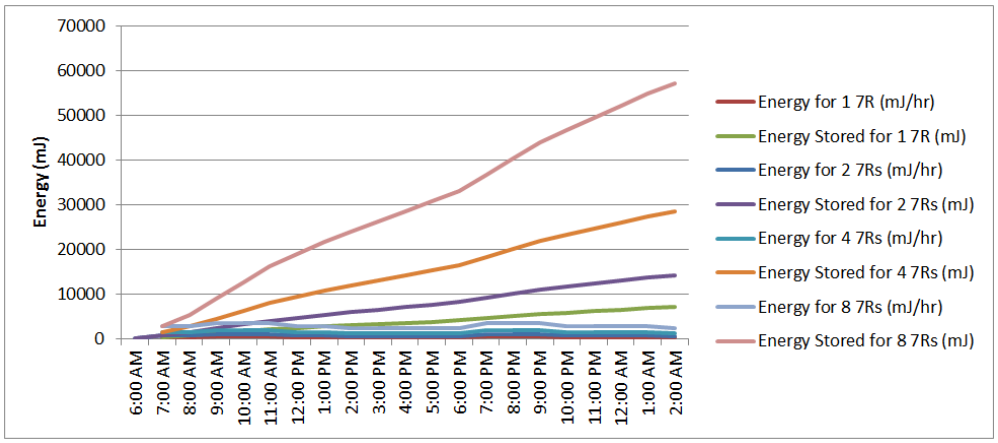

Figure 39- Net energy harvested in the main exit of Sol for different numbers of Thunder 7Rs

In order to support the Cookie Platform, the harvester needs to produce a minimum of 2.3 J per hour in order for the node to just stay asleep. Every event adds about 320 mJ to the power draw, and so with this information the amount of 7R's needed can be visualized in figure 40, which compares the minimum energy that needs to be produced in one hour to support the specific mode to the energy produced per hour for each configuration:

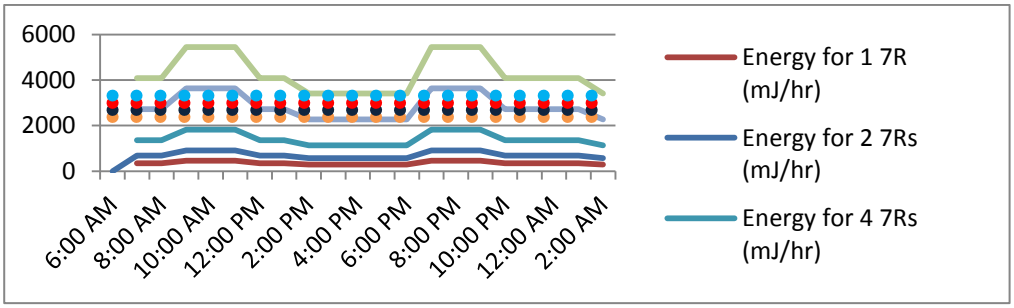

Figure 40- Comparison of the energy rates produced by different numbers of actuators and the minimum needed for different event counts

One can see that a minimum of 8 7R's with the current harvester configuration would be needed to maintain the sleep mode all day; even though it dips below the level between 2 and 6, it will store enough charge during the peak footfall times in order to keep itself alive during the desolate periods. The figures below show the net energy harvested when the Cookie is connected and in various configurations.

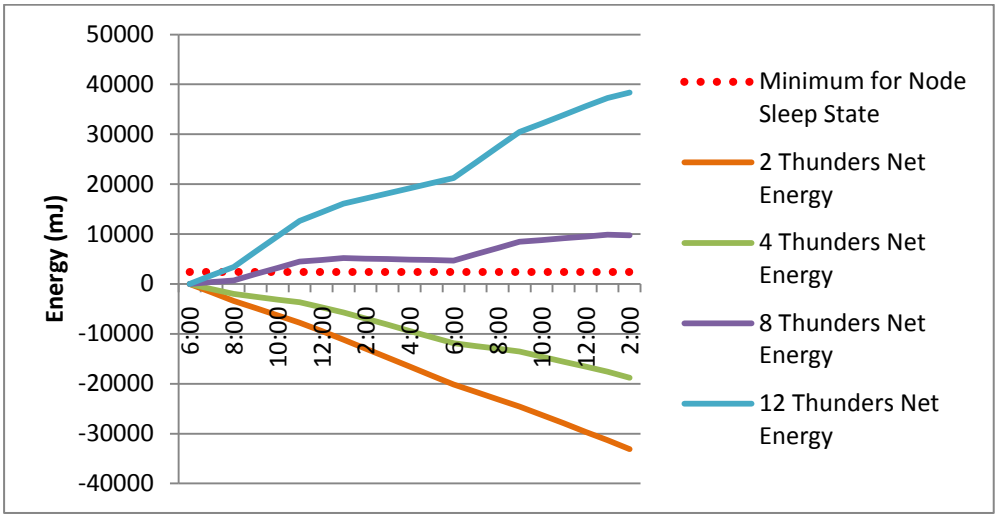

Figure 41- Net energy in the storage elements while supporting sleep mode

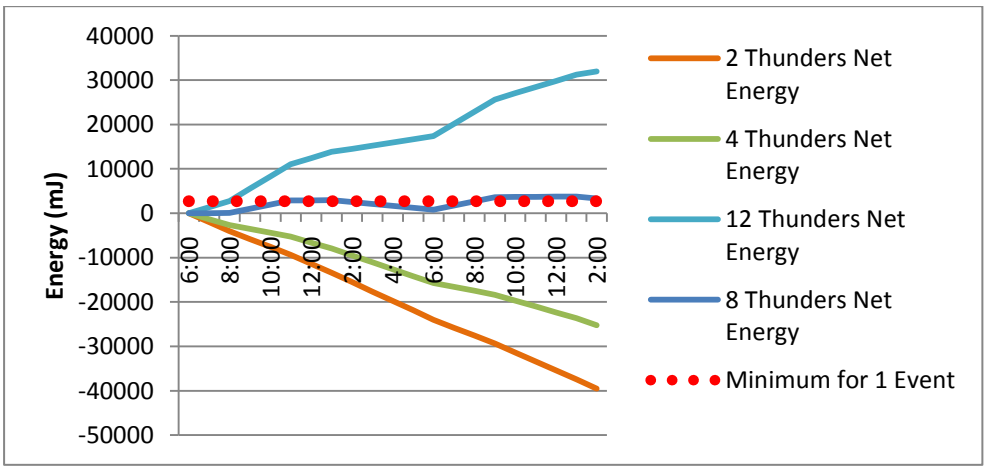

Figure 42- Net energy in storage element while supporting 1 event per hour

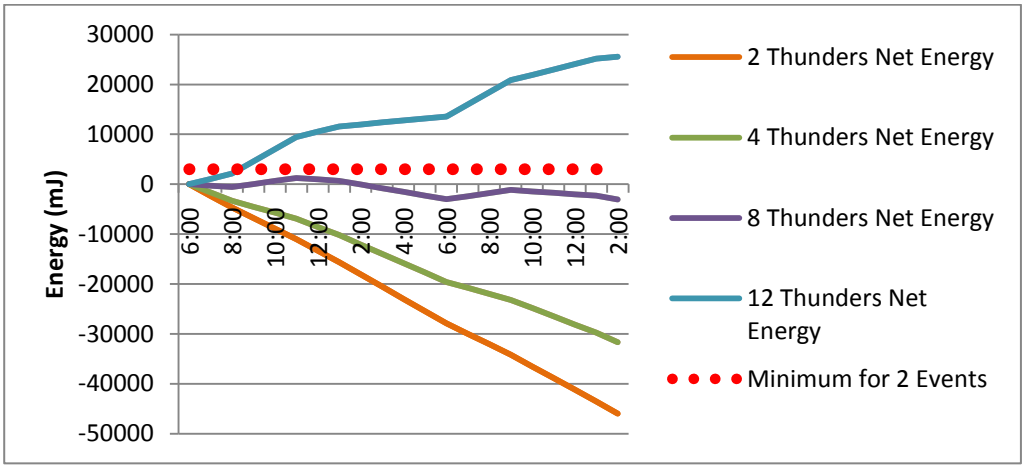

Figure 43- Net energy in storage element while supporting 2 events per hour

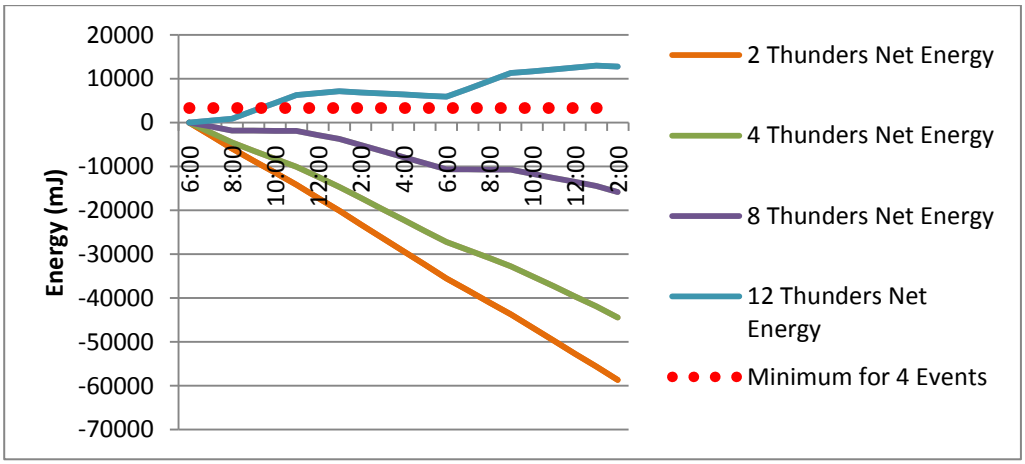

Figure 44- Net energy in storage element while supporting 4 events per hour

One can see that a minimum of 8 Thunders is needed for this application, and that even at 1 event per hour it is only functioning for spurts. One way to overcome this without adding more components is to wait until enough energy has been harvested in the morning before coming online. The plots above assumed that the Cookie would also be drawing power in Sleep Mode as the harvester begins its operation in the morning, which is counterproductive when the harvester cannot produce enough instant energy to keep it running. Although it was found that it didn't make a big difference in the 2 and 4 Thunder configurations (they still couldn't produce enough power to support periodic events with the Cookie), for the 8 Thunder configuration allows it to keep itself operational throughout the rest of the day:

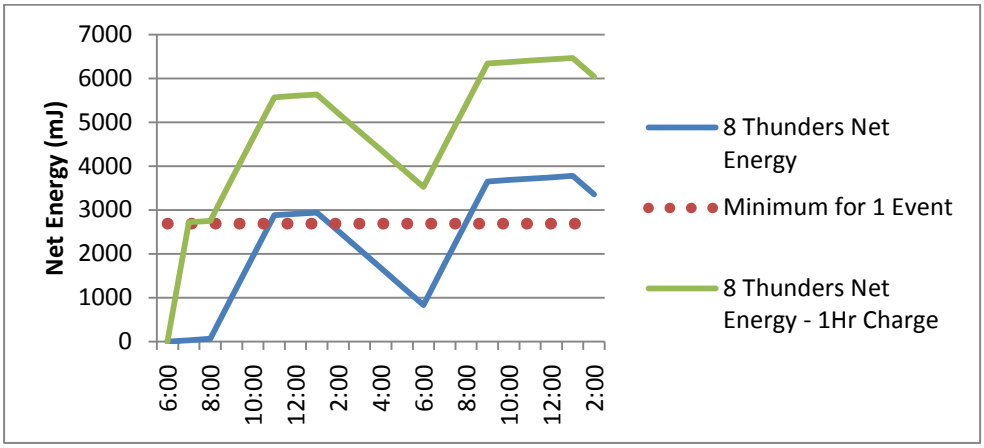

Figure 45- Precharging the storage element for 1 hour can give the node enough of a boost to make it through the rest of the day

This means that if it's okay for the WSN node to be quiet for the first hour of the day to charge up, fewer components can be used. These plots also assume that there is no net charge left over from the previous day, which could easily be the case depending on the application. The same method could be applied in the node algorithm throughout the day—if the energy reaches a critical level at any point (knowing that it would not be able to support another event or even sleeping for the next x minutes, it can shut down the node completely and wait until it has enough energy to support it again. This is a minor inconvenience for the data gathering; if it is very critical data then a good idea would be to use a Li-Ion battery pack as a backup and either charge it with the harvester or charge a supercapacitor to be used in conjunction with the Li-Ion pack. Note that depending on the storage configuration this could mean more maintenance—the backup battery packs would have to be either externally charged or replaced after a while if they aren't being charged by the harvester.

This brief implementation study for the Sol metro reveals that it is indeed possible to have a WSN inside the metro with self-sufficient nodes, and also that special care has to be taken in order to ensure the success of the node. It is rare to have a solution that will work from one place to another—as the specifications of the network change (different sensors, amount of events in an hour, footfall rate, and/or different nodes) the harvester and its power management system needs to be catered to that specific WSN. This solution would need a minimum of 12 Thunder devices (or less if pre-charging is an option or if a net charge is left over from the previous day), which would be a minimum of 1300 euros to build this node.

Existing Products

There exists several companies that are harvesting human energy for use in various systems, and they have designed some very efficient devices that can capture much more energy than this harvester. The two main companies are PaveGen headquartered in London and Energy Floors based out of Rotterdam. The Energy Floors system claims that it can reclaim up to 30% of the energy generated on a dance floor, which is many magnitudes greater than the piezoelectric harvester built in this thesis work. It should be noted that these systems use electromechanical recovery systems and are very costly to not only purchase but also to install and maintain. One study estimates that it would cost about $800,000 for a 7.3 kWh/day, 370 m^2 installation from one of the leading providers. This equates to about $500-600 per tile, plus thousands in maintenance fees[19]. Another quote was for the renting of a much smaller 50-tile, 173 W/day system for 1-3 years. This would cost over $35,000 for the rental and another $30,000 for installation and maintenance[19]. The scalability of these products is strictly limited to expansion in the x and y directions, which isn't always an option. Also, in addition to the added cost of the units, the installation and maintenance fees increase as well. This is where this project could find its niche—in a place where the budget is limited, space is tight, and the application is very low-power such as an environmental sensor contained in a WaspMote or TelosB node.

Figure 46- Visualization of human traffic harvesters used in stairs (Pavegen Systems)

Piezoelectric energy harvesters are already finding their ways into airports, dance floors, roads, museums, and other public places. As we are headed for a future where every subsystem is connected to each other in order to provide a more efficient and intelligent environment, energy harvesters such as this one will be crucial components to make smart cities a reality. This project showed the potential in recovering human footsteps for use in electronic devices, and that even if the energy levels recovered are relatively low, it is cheap to produce and there are a myriad of ultra-low power electronic components and devices that can work at the power levels harvested from the Thunder 7R's. With additional development, especially of the mechanical energy coupling system, this harvester design will yield more energy extracted from the foot traffic and be in a better position to compete with the existing products.

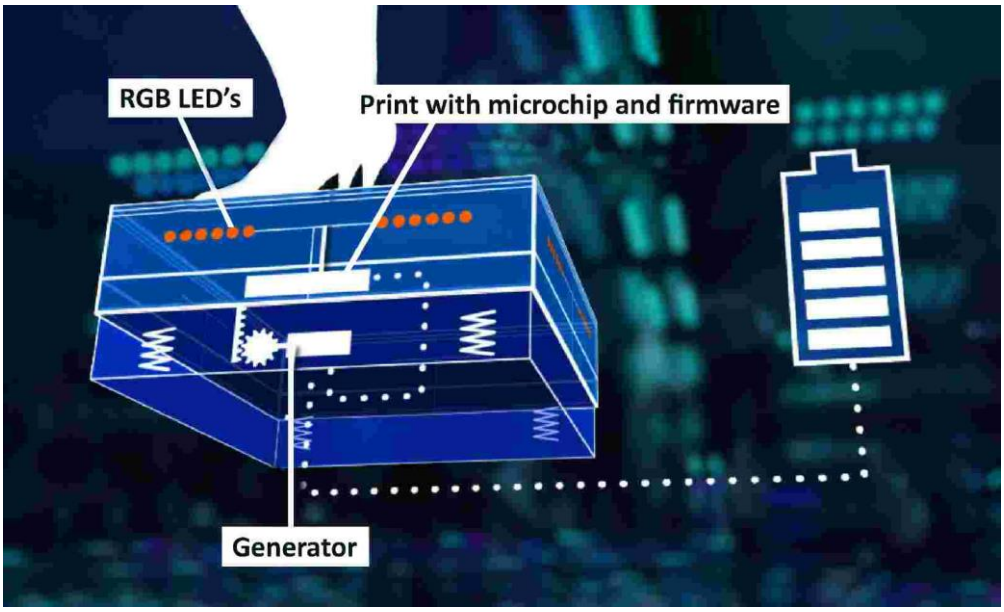

Figure 47- Diagram of electro-mechanical recovery system from an available harvester for a dance club (Energy Floors)

Conclusion

A low-cost piezoelectric energy harvester was designed, built, simulated, and tested with promising results. Even though this device does not produce as much power as the market-available products nor is it nearly as efficient, it produces enough energy for a wide variety of applications due to the advent of ultra-low power electronic components. This would have been nearly impossible without the LTC3639 chip, which is unique in that it can efficiently transform high voltage, low current signals into useable voltage levels. Another great aspect of this project is it's scalability—every 7R that is added (either in a stacked or simply supported configuration) will add approximately a 10 mJ/minute capability under reasonably heavy footfall, and this number will only increase as the mechanical system surrounding the Thunders is refined in order to subtly oscillate after a footfall event to extract even more energy from the actuators. This is a delicate balance, however—when smaller springs were tried with this harvester, the action of the top oscillating up and down proved to be too distracting and dangerous to pedestrians, especially when walking down a set of stairs. The other way to achieve an oscillatory effect is to significantly increase the mass of the top lid, which may or may not be practical in a given situation. As it stands right now, it would cost about 1500 euros to install a self-reliant node in the main exit of the Sol metro station. This is reasonable enough to explore the possibility of installing piezoelectric-based energy harvesters at the Sol metro station to support WSN nodes, especially considering the fact that using lower power nodes such as the TelosB or WaspMote would extend the life or number of sensor readings for a given amount of actuators.

References

[1] Jordi Colomer-Farrarons, Pere Lluis Miribel-Catala, "A CMOS Self-Powered Front-End Architecture for Subcutaneous Event-Detector Devices", 2011 Springer Books

[2] http://mems.caltech.edu/courses/EE40/Class_Notes_Posted/08_Piezoelectricity.pdf

[3] Salem Saadon, Othman Sidek, "Environmental Vibration-based MEMS Piezoelectric Energy Harvester(EVMPEH)", Collaborative Microelectronic Design Excellence Center (CEDEC),

[4] M. Renaud, K. Karakaya, T. Sterken, P. Fiorini, C. Van Hoof, R. Puers, "Fabrication, modeling and characterization of Intelligent Material Systems and Structures, vol. 16, pp. of MEMS piezoelectric vibration harvesters," Sensors and Actuators a-Physical, vol.145, pp. 380-386, 2008.

[5] J. Rastegar, C. Pereira, and H. L. Nguyen,"Piezoelectric-based power sources for harvesting energy from platforms with low frequency vibration - art. no.617101," Smart Structures and Materials 2006

[6] Y.K. Tan Student Member, IEEE, K.Y. Hoe, Student Member, IEEE, and S.K. Panda, "Energy Harvesting using Piezoelectric Igniter for Self-Powered Radio Frequency (1F) Wireless Sensors" SrMIEEE

[7] Rahul Shukla, S. Adam Qaisar and Andrew J. Bell, "Towards the Development of Efficient Low Frequency Piezoelectric Energy Harvesters", Institute for Materials Research, School of Process Environmental and Materials Engineering, University of Leeds

[8] R. W. Schwartz and M. Narayanan, "Development of high performance stress-biased actuators through the incorporation of mechanical pre-loads," Sensors and Actuators A, vol. 101, pp. 322-331, 2002.

[9] S. Meninger, A.P. Amirtharajan and R.Chandrakasan,"Vibration-to-Electric Energy Conversion", IEEE Trans VLSI Syst., vol.9, pp.64-71, 2001.

[10] J. Ajitsaria, *et al.*, "Modeling and analysis of a bimorph piezoelectric cantilever beam for voltage generation," Smart Materials and Structures, vol. 16, pp. 447-454, 2007.

[11] M. J. Guan and W. H. Liao, "On the efficiencies of piezoelectric energy harvesting circuits towards storage device voltages," *Smart Mater. Struct.*, vol. 16, no. 2, pp. 498–505, 2007.

[12] A. Erturk and D. J. Inman, "An experimentally validated bimorph cantilever model for piezoelectric energy harvesting from base excitations,"*Smart Mater. Struct.*, vol. 18, no. 2, art. no. 025009, 2009.

[13] S. M. Shahruz, "Limits of performance of mechanical band-pass filters used in energy scavenging," Journal of Sound and Vibration, vol. 293, pp. 449-461, 2006.

[14] S. Priya, *et al.*, "Piezoelectric windmill: A novel solution to remote sensing," Japanese Journal of Applied Physics, vol. 44, pp. L104-L107, 2005.

[15] J. Lee, Y. Su, and C. Shen, *et al.*, "A comparative study of wireless protocols: Bluetooth, UWB, ZigBee, and Wi-fi" 33rd Annual Conference of the IEEE Industrial Electronics Sociery, November 5-8, 2007.

[16] L. Miller, C. Ho, P. Shafer, P. Wright, J. Evans, R. Ramesh, "Integration of a low frequency, tunable MEMS piezoelectric energy harvester and a thick film micro capacitor as a power supply system for wireless sensor nodes", IEEE Transactions on Ultrasonics, 978-1-4244-289, 2009.

[17] D. Koyama, K. Nakamura, "Array configurations for higher power generation in piezoelectric energy harvesting", 2009 IEEE International Ultrasonics Symposium Proceedings, page 1973.

[18] S. Lee, B. Youn, "A new piezoelectric energy harvesting design concept: multimodal energy harvesting skin", IEEE Transactions on Ultrasonics, Ferroelectrics, and Frequency Control, vol. 58, No. 3, March 2011.

[19] Doyle, Brian, "Piezoelectric energy harvesting" Materials Science and Engineering Department, Rutgers University, May 2012.

[20] Keawboonchuay, C., & Engel, T.G., "Maximum power generation in a piezoelectric pulse generator", IEEE Transactions on Plasma Science, pp. 1879-1885, 2003.

[21] E. Lefeuvre, "Piezoelectric energy harvesting device optimization by synchronous electric charge extraction", Journal of Intelligent Material Systems, Vol. 16, 865-876, 2005.

[22] J. Colomer-Farrarons, "Self-Powered temperature sensor powered by vibration energy harvesting", Proceedings of the 32nd Conference on Design of Circuits and Integrated Systems, 2007.

[23] N. Amore, O. Kanoun, "Investigation to the use of vibration energy for supply of hearing aids", Proceedings of the 2007 IEEE Instrumentation and Measurement Technology Conference, pp. 1-6, May 2007.

[24] Roundy S., "Energy scavenging for wireless sensor nodes with a focus on vibration to electricity conversion", Unpublished Doctoral Dissertation, University of California Berkeley, 2003.

[25] Roundy S., & Wright, P.K., "On the effectiveness of vibration-based energy harvesting", Journal of Intelligent Material Systems and Structures, pp. 809-823, 2005.

[26] Sodano H., Inman D.J., Park G., "Comparison of piezoelectric energy harvesting devices for recharging batteries", Journal of Intelligent Material Systems and Structures, pp. 799-807, 2005.

A special thanks to everyone in the Politécnica de Madrid ETSII department for making my time in Madrid unforgettable, especially my advisers Teresa Riesgo and Pedro Alou, to the Politécnico di Milano Electronics and Information department for supporting me during my research post there, to the University of Connecticut Engineering Department for selecting me to be a part of the EAGLES program, and to my parents, especially my mother, who passed during the writing of this but for whom I owe almost everything to.